Journal of Materials Chemistry B

ROYAL SOCIETY OF CHEMISTRY

PAPER

View Article Online
View Journal

Cite this: DOI: 10.1039/d6tb00315j

Impact of the polymer side chain chemistry on interactions of amino-acid-derived polyelectrolytes with cells

Jonas De Breuck,[a] Theresa M. Lutz,[a] Lena M. Lipka,[a] Christian Jahns,[a] Jonas P. Debbeler,[bc] Valérie Jérôme,[d] Ruth Freitag,[de] Anja Traeger[bcf] and Meike N. Leiske *[ag]

Polyelectrolytes have gained significant attention for their unique, potentially specific association with living cells. Particularly, amino-acid-derived polyzwitterions feature specificity to cancer cells, highlighting their potential for biomedical applications. Here, the synthesis of lysine- and phenylalanine-derived polyelectrolytes *via* post-polymerisation modification is presented. The amidation of activated ester prepolymers with protected basic amino acids and their subsequent deprotection yield tailored amino acid-functionalised polyzwitterions comprising side chain chirality. Similarly, the use of achiral neutral amino acids results in polyanionic analogues of these polyzwitterions. *Via* this strategy, a small library of five polymers was created, which enables the careful evaluation of structure–property relationships of polyelectrolytes and their interactions with cells. In particular, we study the influence of side chain motifs: (i) aliphatic *vs.* aromatic side chains, (ii) permanent *vs.* non-permanent charge, and (iii) zwitterionic *vs.* anionic patterns. High-performance liquid chromatography measurements are performed to investigate the influence of both the charge character and aromaticity on the hydrophilicity of the polyelectrolytes. Response to changes in the pH value is studied by dynamic light scattering (DLS) and electrophoretic light scattering at different pH values. Furthermore, polyelectrolyte stability under biologically relevant conditions, *i.e.* in the presence of model proteins and more complex protein mixtures from foetal bovine serum, is assessed by DLS. Association with cells from different cancer and non-cancer cell lines provides information regarding structural driving forces for association efficiency and specificity. Furthermore, fluorescence imaging shows fast uptake of polyanions into targeted cells, making them interesting candidates for drug-delivery applications.

Received 6th February 2026,
Accepted 11th May 2026

DOI: 10.1039/d6tb00315j

rsc.li/materials-b

1. Introduction

Limited stability of therapeutic compounds and loss of activity upon modification are major drawbacks of conventional medicine.[1,2] One strategy to overcome these limitations is the encapsulation into stable carriers perhaps possessing targeting ligands to facilitate the selective delivery to the target site.[2,3] Besides protecting the drug, these carriers (*e.g.* composed of synthetic polymers) must possess low-fouling properties and cell-specific moieties (*e.g.* proteins, peptides, aptamers, polysaccharides or small biomolecules).[4] Building blocks capable of fulfilling these tasks ought to be identified. The engineering of polyelectrolytes has proven to be a powerful strategy to tailor functional molecules for such biomedical applications. By systematically varying charge density,[5] backbone architecture,[6] and side chain functionality,[7] polyelectrolytes can be designed to control (i) intermolecular interactions such as polymer–protein interactions (*i.e.* reduce aggregation with proteins),[8] (ii) self-assembly to form higher-level structures for stable drug transport in the biological environment, and (iii) responsiveness to external stimuli to facilitate cellular uptake.[9] The latter is important since therapeutic compounds are often cell membrane-impermeable and polyelectrolytes may overcome the membrane barrier efficiently.[10] One way is to harness amino acid transporters – symporters, antiporters (overexpressed in cancer cells) and uniporters – and allow the

[a] *Macromolecular Chemistry, University of Bayreuth, Universitätsstraße 30, 95447 Bayreuth, Germany. E-mail: meike.leiske@uni-bayreuth.de*
[b] *Laboratory of Organic and Macromolecular Chemistry (IOMC), Friedrich Schiller University Jena, Humboldtstr. 10, 07743 Jena, Germany*
[c] *Jena Center for Soft Matter (JCSM), Friedrich Schiller University Jena, Philosophenweg 7, 07743 Jena, Germany*
[d] *Process Biotechnology, University of Bayreuth, Universitätsstraße 30, 95447 Bayreuth, Germany*
[e] *Bayreuth Center for Molecular Biosciences (BZMB), University of Bayreuth, Universitätsstraße 30, 95447 Bayreuth, Germany*
[f] *Department of Pharmaceutical Chemistry, Institute of Pharmacy, Friedrich Schiller University, Philosophenweg 14, Jena, Germany*
[g] *Bavarian Polymer Institute, Universitätsstraße 30, 95447 Bayreuth, Germany*

uptake of anionic, neutral, cationic, or specific amino acid motifs (*e.g.* leucine, phenylalanine, glycine, proline, and cysteine/glutamate), respectively.[11] Thus, amino acid functionalisation of polymers might improve targeting and internalisation by cancer cells compared to non-cancerous cells.[6] After membrane engulfment *via* endocytosis, a rapid release of the therapeutics (*i.e.* endosomal escape) is desired to minimise degradation of the therapeutic compound.[12]

In the literature, non-ionic polymers based on polyethylene glycol (PEG) are described as performant tools for aggregation between proteins and polymer nanocarriers.[13,14] However, tumour cell specificity of PEG itself is comparatively low, thereby calling for decoration with additional targeting ligands (*e.g.* antibodies), which is both costly and time-consuming. The targeting efficiency of non-ionic polymers without these ligands is mostly based on the enhanced permeability and retention (EPR) effect[15] – a passive cell targeting method – which is less efficient in larger tumours due to their cellular heterogeneity and thus, intracellular carrier accumulation is limited.[16] Hence, tumour targeting based on specific natural properties of tumour cells is of high interest. Contrarily to PEGylated carrier systems, polyelectrolytes may be designed to tackle the tumour targeting challenge[17] and show superior suitability for the design of next-generation systems: polyelectrolytes combine synthetic precision with selective binding, controlled release properties, tuneable solubility and biocompatibility.[17,18]

Although classical endocytic pathways such as clathrin-mediated uptake, caveolae-dependent endocytosis and macropinocytosis have been extensively characterised, their applicability to synthetic polyelectrolyte systems remains incompletely understood because polymer–cell interactions are strongly governed by surface charge and interfacial physicochemistry. In contrast to the widely studied cationic delivery vectors, anionic and zwitterionic polymers interact with biological membranes in more subtle ways, often involving weak electrostatic interactions, hydration-layer formation and specific binding to membrane components such as proteins or glycosaminoglycans.[19–22] These interactions can influence adsorption, membrane wrapping and subsequent internalisation processes, yet the mechanistic details remain considerably less explored than that for polycationic systems. Importantly, anionic and zwitterionic polymers are frequently employed to improve biocompatibility, reduce nonspecific protein adsorption and minimise cytotoxicity, owing to their strong hydration and charge-balanced character.[23–26] Despite these advantages, their comparatively weak electrostatic interactions with cellular membranes often result in lower uptake efficiencies and less predictable intracellular trafficking, highlighting a key limitation of current materials. Moreover, the relationship between polymer architecture, charge distribution and biological response remains insufficiently resolved, particularly for zwitterionic or charge-regulated macromolecules. Consequently, while cationic polymers have historically dominated studies of polymer-mediated delivery, the development of anionic and zwitterionic polyelectrolytes capable of precisely modulating polymer–membrane interactions represents an important emerging direction for improving cellular compatibility while maintaining effective intracellular transport.

For example, Fuji *et al.* showed that certain polyelectrolyte building blocks, namely zwitterionic polybetaines and amino-acid-derived polyzwitterions can actively accumulate in tumours.[27,28] They pass the cell membrane by transporter-mediated mechanisms, which offer a new platform for targeted, biocompatible cancer nanomedicine. In addition, amino-acid-derived polyelectrolytes show beneficial features based on their biomimetic properties.[17,18] Thus, these polymers have *e.g.* antifouling properties due to their high charge density and strongly bind to a hydration layer *via* electrostatic interactions.[29] This layer is much more stable than the one associated *via* hydrogen bonding with non-ionic polymers (*e.g.* poly(*N*-acryloylmorpholine) (PNAM) or PEG)[30,31] since it forms a significant barrier that biomolecules must overcome before attaching directly to the polymers.[32] Moreover, the properties of polyelectrolytes can be tuned by their side chain hydrophobicity,[33,34] counter ions[35] and backbone chemistry[6] to govern stable polymer performance and transportation in the body at physiological pH values (7.4), while triggering intracellular release mechanisms such as endosomal escape at acidic pH levels (5.0–6.8).[36] Hence, the functionality of polyelectrolytes can be used for introduction of targetability and transmembrane transfer efficiency, which are important tools to modulate a polymer (complex) for potential medical applications such as drug delivery, gene transfection, and tissue engineering.[37,38] Synthetically, the design of polyelectrolytes from amino acids is a widely explored field, see, *e.g.* the recent review on the synthesis and polymerisation of amino acid-derived monomers by our group.[39] Studies have furthermore shown that lysine- and ornithine-based brushed polyelectrolytes show low fouling behaviour as they did not show any aggregation towards undiluted serum for 24 h. Furthermore, pH- and temperature responsiveness has been observed for isoleucine- or leucine- and serine-based polymers, which are interesting functionalities for various applications as stated above.[40,41] We previously explored the introduction of permanent positive charges in the polymers to generate zwitterions with a fixed cationic centre. With that, we stabilised the zwitterionic character over a wider pH range.[42]

Driven by our previous study, which examined the impact of the backbone chemistry of amino-acid-derived polyzwitterions on their cellular specificity, we now investigated the effect of the side chain chemistry as well as alterations to the ionic moiety itself. Similar attempts were previously pursued by Fujii *et al.*, where the internalisation of various polymethacrylamides into cancer cells was studied. These authors showed that their cytocompatible polymers were actively taken up by cancer.[37] Inspired by these observations, our research aims to enhance the comparability between the developed polymer systems. We intended to achieve this by synthesising polyelectrolytes using activated esters as precursors, thereby mitigating the influence of the degree of polymerisation (X_n) and dispersity ($Đ$) on the final product. We were interested in the influence of the positive charge (presence/absence) and hydrophobicity (aromatic/alkyl-side chain) on protein and cell interactions. Therefore, a small library was created where different amino acid or amino-acid-like structures are substituted in the side chain to

obtain zwitterionic or anionic analogue amino acid-derived polyelectrolytes. To summarise, this study aims to elucidate how charge (zwitterionic/anionic), side chain hydrophobicity (aliphatic/aromatic groups) and persistent positive charge influences physicochemical parameters. To obtain this information, the cell association (flow cytometry) and cellular uptake (confocal laser-scanning microscopy) of polyelectrolytes to cancer and non-cancer cells was investigated in a comparative manner. Competitive inhibition assays were applied to study the uptake mechanism further. The systematic variation of side chain building blocks and their influence on cellular interactions provide insights for the development of novel polyelectrolytes for biological applications.

2. Results and discussion

2.1. Synthesis and characterisation of amino-acid-derived polyelectrolytes

Aiming to investigate the side chain chemistry of amino-acid-derived polyelectrolytes and their interaction with biological matter (*i.e.* the nature of the zwitterion as well as the spacer between the ionic group and the polymer backbone), we synthesised polyelectrolytes *via* post-polymerisation modification (PPM) of poly(*N*-acryloyl succinimide) (PNAS). Here, PNAS was obtained from reversible addition–fragmentation chain transfer (RAFT) polymerisation and subsequently reacted with different amino acids to design three different polyzwitterions: (i) an aliphatic spacer and a permanent positive charge, (ii) an aliphatic spacer and a non-permanent positive charge, and (iii) an aromatic spacer and a non-permanent positive charge as well as two corresponding polyanions with (iv) aliphatic and (v) aromatic spacers (Scheme 1).

Consequently, the PPM of PNAS with five different reagents was conducted: (i) Me_3Lys-OMe-NH_2,[42] (ii) *N*-Boc-lysine-OH (Boc-Lys-OH),[42] (iii) Boc-4-aminophenylalanine (Boc-4-AmPhe-OH), (iv) 6-aminohexanoic acid (6-AmHex-OH), and (v) 3-(4-aminophenyl)propanoic acid (4-AmPhenylPr-OH). The successful PPM was verified *via* ^{1}H NMR measurements, showing the disappearance of the characteristic peak of NAS at δ = 2.8 ppm after the reaction, indicating full conversion (Fig. 1A, B and Fig. S1). In the case of the aliphatic polymers P(Me_3Lys-OMe-AAm), P(Boc-Lys-OH-AAm), and P(Hex-OH-AAm) a peak shift

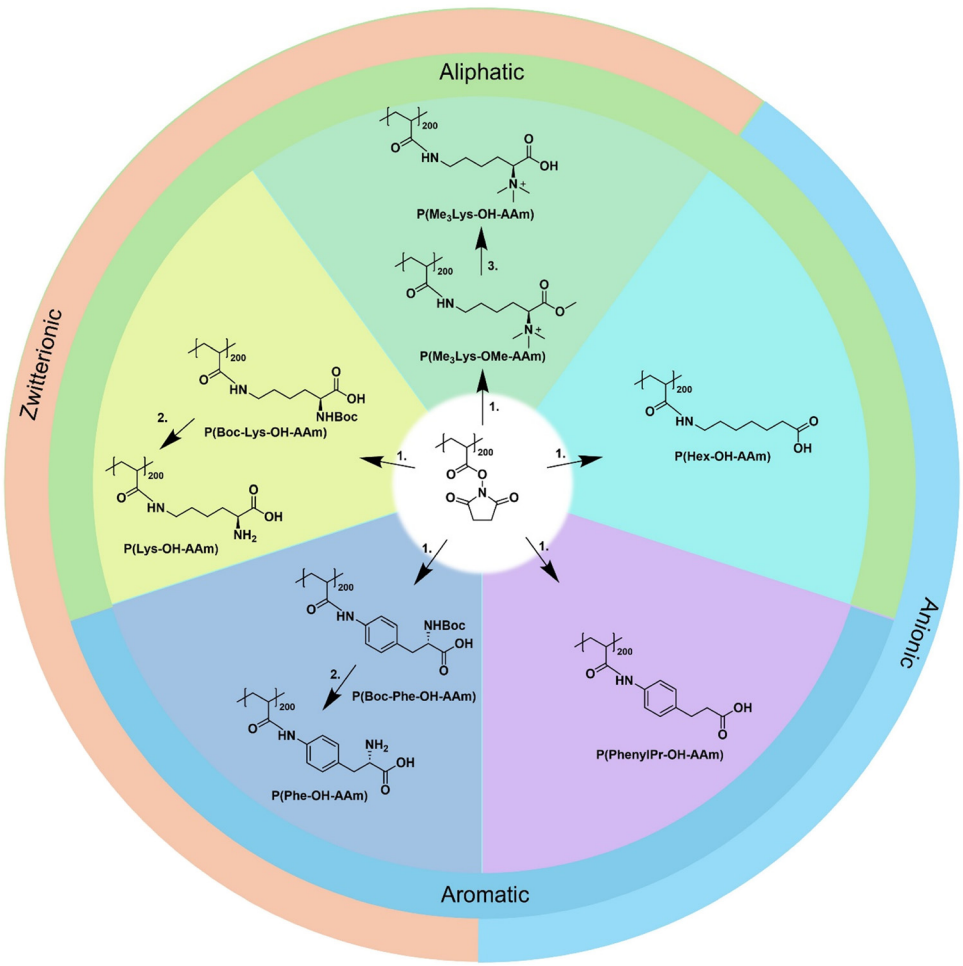

Scheme 1 Synthesis of P(Boc-Lys-OH-AAm), P(Me_3Lys-OMe-AAm), P(Hex-OH-AAm), P(Boc-Phe-OH-AAm) and P(PhenylPr-OH-AAm) *via* PPM. (1) Et_3N, DMF and Boc-Lys-OH, Me_3Lys-OMe-NH_2, 6-AmHex-OH, Boc-4-AmPhe-OH and 4-AmPhenylPr-OH, respectively. 24 h at room temperature. (2) 50 : 50 v/v% (TFA/H_2O), overnight at room temperature. (3) 0.1 M NaOH, 24 h at room temperature.

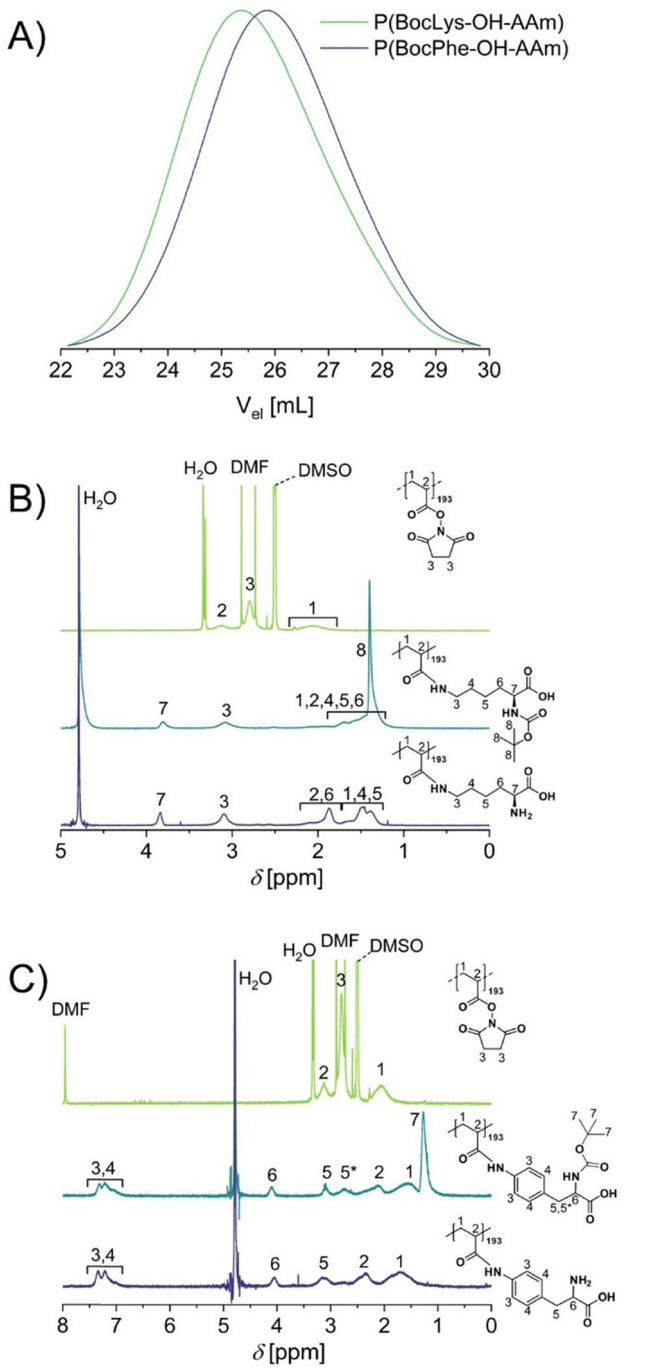

Fig. 1 (A) Size-exclusion chromatograms (0.07 M aq. Na_2HPO_4) of P(Boc-Lys-OH-AAm) (green) and P(Boc-Phe-OH-AAm) (blue). (B) ^{1}H NMR spectra (300 MHz) of poly(*N*-acryloyl succinimide) (green, DMSO), P(Boc-Lys-OH-AAm) (cyan, D_2O) and P(Lys-OH-AAm) (blue, D_2O). (C) ^{1}H NMR spectra (300 MHz) of poly(*N*-acryloyl succinimide) (green, DMSO), P(Boc-Phe-OH-AAm) (cyan, D_2O) and P(Phe-OH-AAm) (blue, D_2O).

from δ = 2.8 ppm in the ^{1}H NMR spectra of the starting compounds (Fig. S2) to δ = 3.0 to 3.1 ppm in the polymer ^{1}H NMR spectra (Fig. 1A and Fig. S1) is observed. This indicates a change in the environment for the methylene group adjacent to the amine (H3), now positioned adjacent to the amide (Fig. S1 and Fig. S2). The aromatic polymers P(Boc-Phe-OH-AAm) and P(PhenylPr-OH-AAm) are characterised by the broadened aromatic peaks compared to the ^{1}H NMR spectra (Fig. 1C and Fig. S1). This shows the different chemical environment each aromatic peak has, something typically observed in ^{1}H NMR spectra of polymers and therefore complementary to disappearance of the characteristic NAS peak (Fig. S3), confirming successful PPM.

The zwitterionic polymers P(Lys-OH-AAm) and P(Phe-OH-AAm) were obtained by acidic deprotection of P(Boc-Lys-AAm) and P(Boc-Phe-OH-AAm). Successful deprotection was verified *via* ^{1}H-NMR as the Boc group signal at δ = 1.4 ppm disappeared (H8 and H7, respectively, Fig. S4 and S5). P(Me_3Lys-OH-AAm) was obtained from P(Me_3Lys-OMe-AAm) after basic hydrolysis as previously shown.[42]

Aqueous size exclusion chromatography (SEC) measurements were conducted to obtain information about the integrity of the polymer chain during the PPM and deprotection and to verify the absence of unwanted chain coupling (*e.g.* caused by aminolysis of the chain-transfer agent (CTA)). All polymers showed monomodal molar mass distributions (Fig. S6 and S7). Deprotection changed the dispersity ($Đ$) of P(Lys-OH-AAm) significantly from 2.25 to 3.27, which was probably caused by the increased charge density and thus the enhanced interaction with the stationary phase of the column. This also resulted in a significantly later elution time and therefore high decrease in apparent molar mass ($M_{n,app}$) from 17.2kDa to 2.0 kDa. This effect was not observed for P(Phe-OH-AAm), where $Đ$ was constant (2.47 to 2.14), which can indicate that the aromatic groups prevent interactions with the stationary phase. Both polymers, however, exhibited monomodal molar distributions (Fig. S8) Generally, all polymers showed increased $Đ$, with $2.0 < Đ < 3.3$, compared to PNAS ($Đ$ = 1.9, Table 1). This broadening may be attributed to the use of a more polar eluent and high density of charged groups in the polymers, which promote hydrogen bonding and ionic interactions with the stationary phase, leading to broadening. Generally, the discrepancies between $M_{n,app}$ and the theoretical molar mass ($M_{n,theo}$) derived from NMR and SEC (Table 1) resulted from the calibration. While $M_{n,theo}$ refers to the mean value derived from

Table 1 Polymer characteristics

Polymer	M^a [Da]	$X_{n,theo}{}^b$	$M_{n,theo}{}^b$ [kDa]	$M_{n,app}{}^c$ [kDa]	$Đ^c$	$t_{ret}{}^d$ [min]
P(Lys-OH-AAm)	200.24	193	38.5	1.9	3.27	11.80
P(Me_3Lys-OH-AAm)	243.33	188	46.5	10.7[e]	1.96[e]	11.75
P(Hex-OH-AAm)	185.22	193	35.6	16.5	2.30	14.49
P(Phe-OH-AAm)	234.25	193	45.0	13.0	2.14	11.97
P(PhenylPr-OH-AAm)	219.24	193	42.1	11.0	2.71	15.94

[a] Molar mass (M) of repeating unit (RU) after deprotection. [b] $X_{n,theo}$ and $M_{n,theo}$ were calculated from ^{1}H-NMR. [c] $M_{n,app}$ and $Đ$ were determined by aqueous SEC measurements (0.07M Na_2HPO_4) on a Suprema column set (PMA standard). [d] t_{ret} was obtained from HPLC using a reversed phase column with a water/acetonitrile mixture + 0.1 vol% trifluoroacetic acid as an eluent. [e] Determined by aqueous SEC measurements (80/20 V% [H_2O/ACN] + 0.1 M NaCl + 0.3% TFA) on a Novema column set (P2VP standard).

the $X_{n,theo}$, which was obtained from conversion of the PNAS precursor, $M_{n,app}$ refers to the calibration standard of the aqueous SEC (*i.e.* P2VP or PMA).

In addition, the cyanine-5 (Cy5)-labelled polymers (*i.e.* P(Lys-OH-AAm)-Cy5, P(Me_3Lys-OH-AAm)-Cy5, P(Hex-OH-AAm)-Cy5, P(Phe-OH-AAm)-Cy5 and P(PhenylPr-OH-AAm)-Cy5), which were required for cell association and internalisation experiments, were synthesised *via* sequential PPM with Cy5-amine and the respective amino acids. Those polymers were analysed as described above and the absence of unbound dye was verified by SEC measurements (Fig. S9 and S10).[6]

2.2. pH-responsiveness and hydrophobicity

The application of polyelectrolytes in biological environments necessitates knowledge about their physicochemical properties, *i.e.* their hydrophobicity and responsiveness to changes in the pH value, which are important driving forces for interactions with cells and proteins. The Cy5-labelled polymers were subjected to high-performance liquid chromatography (HPLC) measurements to gain information about their relative hydrophobicity (Fig. S11). Under eluent conditions (pH 2) – chosen so the ionic state around the pK_a of the polymers cannot influence the elution time – the anionic polymers P(PhenylPr-OH-AAm)-Cy5 (polymeric retention time (t_{ret}) $\sim$ 16 min) and P(Hex-OH-AAm)-Cy5 (t_{ret} $\sim$ 15 min) were the most hydrophobic (Table 1, Fig. 2A and Fig. S11). This increased hydrophobicity is explainable by the protonation of the carboxylic acids[36] as the pH is below the reported pK_a (pH 4.88 for hexanoic acid and 4.37 for 3-phenylpropanoic acid).[43] Furthermore, it was shown that the aromatic side chain influences the hydrophobicity of the polyanions. It is assumed that aromatic spacers feature an increased hydrophobicity due to the higher polarisability of the aromatic rings inducing stronger London dispersion forces with the C18 chains than a flexible alkyl group of similar size on the reversed phase column. In contrast, the zwitterionic polymers, P(Lys-OH-AAm)-Cy5, P(Me_3Lys-OH-AAm)-Cy5 and P(Phe-OH-AAm)-Cy5, showed a similar t_{ret} of $\sim$12 min. Hence, side chain aromaticity or permanent positive charge has no influence on the hydrophobicity of zwitterionic polymers at pH 2.0. Moreover, we calculated the theoretical partition coefficient (log P) to obtain numerical values for comparison with the experimental data (Fig. S12). All polymers except P(Lys-OH-AAm) exhibit a positive theoretical log P value, which emphasizes the hydrophobic character of the polymers corroborating the HPLC data. Only P(Lys-OH-AAm) showed a negative theoretical log P value of -0.2319, indicating a slightly hydrophilic character. This could be attributed to the fact that the computational data are based on monomer calculations (one repeating unit per polymer). The algorithm of the trained machine learning model is designed for small molecules;[44] hence complete polymers were excluded from the calculation of theoretical log P values and future application of algorithms for polymer-based systems could improve accuracy.

To support these findings, the effect of the pH on self-assembly was studied using dynamic light scattering (DLS) measurements performed at different pH values to get a general overview of its solubility behaviour (Fig. 2B, Fig. S13 and S14). Additionally, changes in particle size serve as an indirect indicator of increased hydrophobicity, as hydrophobic interactions are expected to dominate upon protonation. This behaviour may be particularly important under biologically relevant pH conditions (pH 6.0–7.5), even though the tested pH values exceed this range to give a general overview of physicochemical properties. With DLS measurements, we confirmed the decreased solubility of the polyanions by number

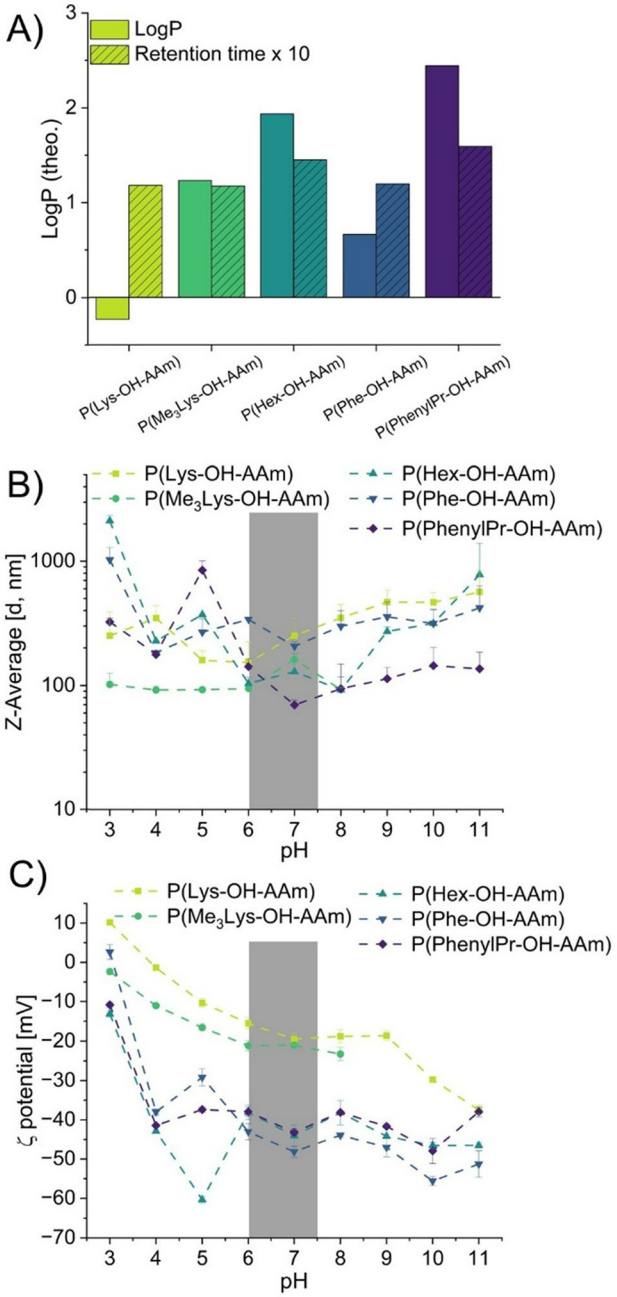

Fig. 2 (A) Partition coefficients and retention time (×10) of the polyelectrolytes. (B) Intensity weighted sizes and (C) ζ-potential of 2 mg mL^{-1} aqueous solutions at indicated pH values. Grey boxes in (B) and (C) indicate the biologically relevant pH range.

size distributions (Fig. S13). For example, P(Hex-OH-AAm) showed hydrodynamic diameters (D_h) of > 1 000 nm at pH 3.0 and $D_h \approx 100$ nm at pH 4.0 and 5.0. Moreover, number size distributions of P(PhenylPr-OH-AAm) showed a D_h between 1 and 10 nm at pH values between 6 and 11, as well as $D_h \approx 100$ nm at pH 3.0 and 4.0. At pH 5.0, in comparison, the largest particles were present with diameters larger than 1000 nm. Visually, we could also see aggregation in the polymer solutions at pH values between 3 and 5 for P(Hex-OH-AAm) and P(PhenylPr-OH-AAm) (Fig. S13). Visual observation of the polymer solutions showed increased turbidity (Fig. S15) for those polymers at low pH values. Those scenarios could be explained by the pK_a values of hexanoic acid and 3-phenylpropanoic acid, which are 4.88 and 4.37, respectively.[43] Both values are close to the pK_a values of P(Hex-OH-AAm) and P(PhenylPr-OH-AAm), respectively, since the amide functional groups do not significantly influence the lower pK_a. As the polyanions are partially and fully protonated, around and below their pK_a, it is also in agreement with our visual observation of aggregates and particle formation in light scattering measurements. The zwitterionic P(Lys-OH-AAm) showed an average particle diameter of around 10 nm across the whole measured pH range from pH 3.0 to pH 11.0, which was visually observed as a transparent solution. However, for the zwitterionic polymers with an aromatic motif in the side chain and permanent positive charge, aggregation was observed at pH 6.0 to 7.0 (P(Phe-OH-AAm)) and pH 7.0 (P(Me3Lys-OH-AAm)) with D_h = 20 to 100 nm and $D_h \approx$ 160 nm, respectively.[45]

Additionally, ζ-potential measurements using electrophoretic light scattering (ELS) provided an insight into the surface charge of the polymers. ELS measurements (Fig. 2C) showed that the zwitterionic amino acid side chains possessed a positive charge at pH 3.0 due to both the protonated carboxy group and the amine protonation at low pH values. This character changes to an overall negative net charge when the pH is raised to 4.0 or higher as both functional groups are deprotonated, and thus, the carboxyl group is present as an anion. The measurements for P(Lys-OH-AAm) are also in agreement with previous data of our group. We found that the isoelectric point (pI) is around pH = 4.3, which could be estimated by the expected pK_a. Previously derived amino-acid-derived polyzwitterions from the literature show similar values.[6,40,42] For P(Phe-OH-AAm), however, the pI observed by ELS was between pH 3.0 and 4.0, which is considerably lower than that of the amino acid phenylalanine, which is approximately at pH = 5.5.[46] The lower apparent pI of P(Phe-OH-AAm) observed by ELS compared to free phenylalanine may result from preferential exposure of carboxylate groups at the particle surface, yielding a negative zeta potential at lower pH values. The aggregation detected by DLS near pH 6.0–7.0 further indicates that the polymer attains maximal hydrophobicity around the expected pI.

The side chains in both P(Hex-OH-AAm) and P(PhenylPr-OH-AAm) only possess carboxyl groups that are mostly deprotonated. Even at pH 3.0, the particles were still negatively charged. But the moderate negative ζ-potentials at pH 3.0 (~ -10 mV) for both acid side chains indicated that most of the carboxyl acid groups were protonated and thus neutral. This results in a less negatively charged dispersion with reduced hydrophilic behaviour, which can also be observed by the increased particle size of these polymers (from D_h 1–10 nm to $\approx$100 nm) during DLS measurement at the respective pH values (pH 3.0–5.0) (Fig. S13C and E). It has already been shown that aggregation into larger structures under mildly acidic conditions, similar to extracellular pH values at tumour sites (pH $\approx$ 6.6),[47] can enhance retention within the tumour tissues as long as they exhibit a small hydrodynamic diameter under physicochemical conditions.

2.3. Interaction of amino-acid-derived polyelectrolytes with proteins

Our previous work demonstrated that both P(Lys-OH-AAm) and P(Me_3Lys-OH-AAm) exhibited a minimal tendency for protein fouling when tested with model proteins such as lysozyme and bovine serum albumin (BSA) in Dulbecco's phosphate-buffered saline (DPBS) solution (pH 7.4).[42] Here, similarly, BSA was chosen as a negatively charged model protein which is mainly present in serum, while lysozyme represented a positively charged model protein and tested in DPBS solution. The effect of foetal bovine serum (FBS) was briefly tested to exclude the formation of sediments.

DLS measurements were performed with the chosen model proteins in DPBS at 37 °C for 24 hours (Fig. 3, Fig. S16 and S17). Before starting the measurement, the protein solution was mixed with the respective polymers P(Lys-OH-AAm), P(Me_3Lys-OH-AAm), P(Hex-OH-AAm), P(Phe-OH-AAm), and P(PhenylPr-OH-AAm). Based on our previous results, it was expected that there would be strong interactions of the polyanions, P(Hex-OH-AAm) and P(PhenylPr-OH-AAm), with the positively charged lysozyme.[5] A sudden increase in size for most of the polymers upon mixing with lysozyme was observed (Fig. 3 and Fig. S16). P(Hex-OH-AAm), however, remained stable (*e.g.* no aggregation observed) over the measured period of 24 h while P(PhenylPr-OH-AAm) immediately formed large aggregates resulting in visible sedimentation at the bottom of the cuvette. Consequently, (almost) no particles were measured at the remaining time points as the sediment did not diffuse through the incident laser beam. For the other polymers, a decrease in particle size over time was further observed, indicating the formation of stable complexes, potentially mediated by the ionic charge of the carboxylate group. When looking at BSA, a negatively charged protein with hydrophobic binding pockets (*i.e.* comprising aromatic amino acid residues), a different image was shown. Here, mainly the aromatic polymers P(Phe-OH-AAm) and P(PhenylPr-OH-AAm) aggregated with the protein into stable particles with a mean diameter above 100 nm, while of the aliphatic polymers solely PMe_3Lys-OH-AAM) showed some minor aggregation (Fig. 3 and Fig. S17). This is in line with previous findings from our group and other studies investigating zwitterionic polymers.[42,48] However, it is noteworthy that aromatic pi–pi interactions seem to surpass electrostatic interactions. This trend will be investigated in greater detail

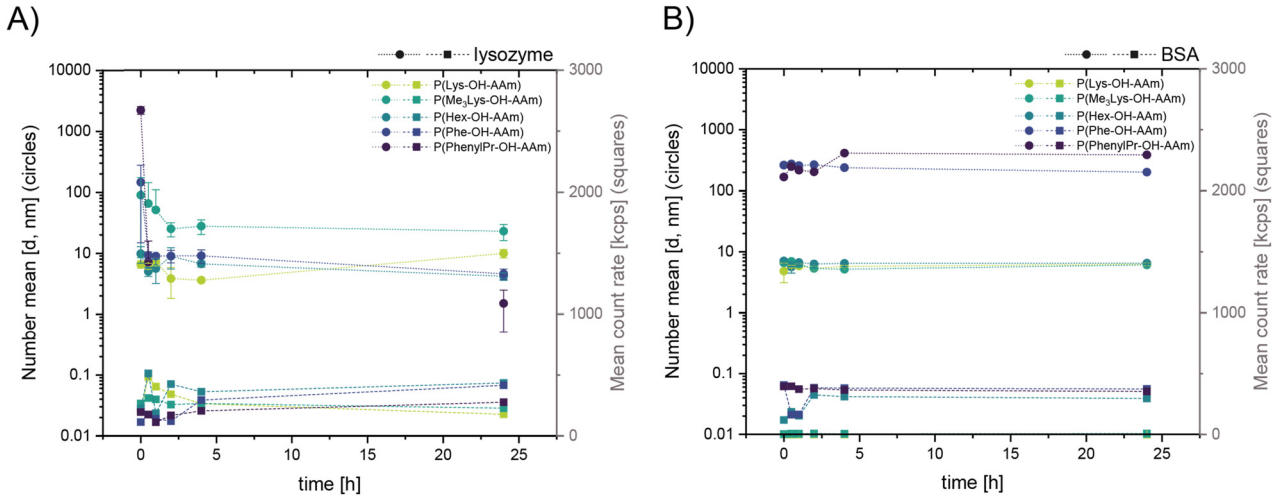

Fig. 3 Time-dependent number size distribution of mixtures of (A) lysozyme and (B) BSA with indicated polymers. The concentration of polymers and proteins was 0.5 mg mL^{-1} each in DPBS. Sizes were analysed by DLS measurements at 37 °C. Values represent the mean and SD of five measurements with three runs each. Lines are to guide the eye and do not represent measured values. All measurements of the polymers with and without proteins can be found in the SI.

in the future. The results related to the aliphatic polyelectrolytes polymers confirm the general trend that zwitterionic polymers or surfaces exhibit excellent resistance to biofouling, thereby being able to improve biocompatibility of coupled materials or cargo (*i.e.* drugs).[29,49–51]

The interesting observation of non-aggregating aliphatic polyanions and instantly aggregating aromatic polyanions in DPBS at 37 °C could possibly be explained by their hydrophobicity, which is related to the HPLC and pH dependent DLS measurements for these polymers (Fig. S11, S13 and S14) and compared to the ones shown in our previous work.[5] There, the more hydrophilic P(Gly-OH-AAm) showed smaller aggregates with lysozyme ($D_h \approx 150$ nm), whereas the more hydrophobic, P(Nva-OH-AAm), showed the formation of larger (although stable) aggregates in combination with lysozyme ($D_h \approx 700$ nm). Comparing t_{ret} values obtained by HPLC, *e.g.* t_{ret} of P(Hex-OH-AAm) (t_{ret} = 14.5 min) and P(PhenylPr-OH-AAm) (t_{ret} = 15.9 min) with P(Gly-OH-AAm) (t_{ret} = 13.2 min) and P(Nva-OH-AAm) (t_{ret} = 16.3 min), we observed a similar retention time for P(PhenylPr-OH-AAm) and P(Nva-OH-AAm), while P(Hex-OH-AAm) has a retention time between P(Nva-OH-AAm) and P(Gly-OH-AAm). Relating the fouling behaviour of the polyanions to their relative hydrophobicity is the most straightforward explanation for the immediate aggregation of the aromatic, more hydrophobic P(PhenylPr-OH-AAm). In comparison, the hydrophobicity of P(Hex-OH-AAm) is insufficient to induce aggregation with lysozyme. Building on these findings, further fouling experiments were conducted in DPBS containing 10% FBS to evaluate potential polymer aggregation under biologically relevant conditions that are later used during *in vitro* experiments. Here, the absence of an increase in particle size, over a measurement time of 5 h, suggests that no polymer–protein aggregation occurs over the period in which cell association experiments will be performed (data not shown).

2.4. Specificity of amino-acid-derived polyelectrolytes to cancer cells

As the main aim of this study was to evaluate the cellular interactions of amino-acid-derived polyelectrolytes based on their side chain chemistry (*i.e.* the nature of the side chain spacer and the ionic moiety), comparative cell association studies were conducted. Here, three exemplary cell lines were chosen: (i) MDA-MB-231 and (ii) HCC-78, two cancer cell lines of different origin, as well as (iii) MCF10A and as tissue-matched control cell line for MDA-MB-231. MDA-MB-231, a breast cancer cell line, was studied previously in our group,[6,52,53] while HCC-78, a lung cancer cell line, served the purpose of expanding the cancer cell toolbox to exclude that the observed effects were attributed to MDA-MB-231 only.

All polymers were tested towards their cytocompatibility using MDA-MB-231 breast cancer cells by performing a 3-(4,5-dimethylthiazol-2-yl)-2,5-diphenyltetrazolium bromide (MTT) assay (Fig. S18). All synthesised polymers were well tolerated by MDA-MB-231 cells at concentrations up to 1 mg mL^{-1} (≙ 25 μM) for 24 h. Moreover, these results were in line with our former study on amino-acid-derived polyanions where the cell viability was consistently ≥70% for concentrations up to 0.1 mg mL^{-1}, ref. 5 and demonstrate that cellular tolerance is unaffected by the side chain spacer (aliphatic or aromatic), or the ionic character ((permanent) zwitterion or anion) of the polymer.

To analyse the cell association of the polymers, the different cell lines were incubated with the Cy5-labelled polymers. To ensure the absence of the cytotoxic effect, a concentration 10-fold lower than the maximum tested concentration in the MTT assay was used (*i.e.* 0.1 mg mL^{-1} ≙ 2.5 μM). Based on the concentration-dependent association experiments, ranging from 0.04 to 2.5 μM, with P(Lys-OH-AAm)-Cy5 and MDA-MB-231 (Fig. S19), a concentration of 2.5 μM was determined to be suitable for further comparative studies as it resulted

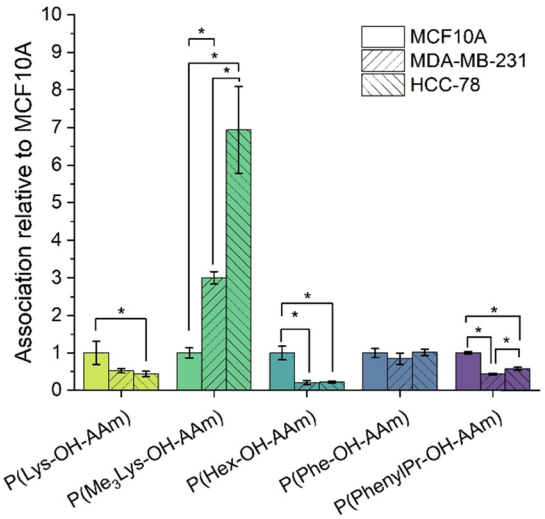

Fig. 4 Cellular association of polymers relative to MCF10A determined by flow cytometry. The cells were seeded in 24-well plates (seeding density for each cell line in the experimental section) and incubated with 2.5 μM polymer solutions (500 μL of FBS-containing cell culture media) at indicated temperatures for 4 h. Values represent mean and SD (n = 4). Statistical analysis (unpaired Welch's t-test) * indicates a significance of $p < 0.05$.

in a sufficient fluorescence signal in MDA-MB-231 breast cancer cells.

The cellular association experiments of all polymers were performed on HCC-78 and MDA-MB-231 and MCF10A.[54] Quantitative evaluation was performed using flow cytometry. PNAM-Cy5 served as internal standard to determine the relative association with different cell types (Fig. S20A), as it has been reported that there is only unspecific association between cancer cells and non-ionic polymers.[6,42,53] As we were mainly interested in the targetability of cancer cell lines by these amino-acid-derived polyelectrolytes we further compared the association amongst the different cell lines, *i.e.* in relation to MCF10A (Fig. 4), which will be discussed in the following.

Generally, comparison with HCC-78 and MDA-MB-231 cells showed a statistically significant difference ($p < 0.05$) between association for P(Me_3Lys-OH-AAm)-Cy5 and P(PhenylPr-OH-AAm)-Cy5 while all other polymers showed similar association behaviour to lung and breast cancer cells. Here, the association of P(Me_3Lys-OH-AAm)-Cy5 with MDA-MB-231 was approximately twice as high as with HCC-78. The cell association of P(Lys-OH-AAm)-Cy5, P(Hex-OH-AAm)-Cy5 and P(Phe-OH-AAm)-Cy5 between those two cancer cell lines did not differ significantly. Differences in the cellular association of polyelectrolytes with different cancer cell lines may be attributed to their surface charge[55,56] or receptor density[57] and provide valuable information about the importance to investigate various cell types to obtain a broader understanding of the driving forces of cell specificity. Future studies shall investigate these differences in greater detail.

Here, we next compared the interaction of the polyelectrolytes with non-tumorigenic human breast cells (MCF10A). The interaction between the permanently, positively charged P(Me_3Lys-OH-AAm)-Cy5 and MCF10A was determined to be statistically significantly lower compared to the cancer cells ($p < 0.05$) (Fig. 4). In contrast, the zwitterionic polymer variant P(Lys-OH-AAm)-Cy5 showed an ~2-fold higher association with MCF10A cells. However, this was not statistically significant compared to cancer cells of the same tissue type (*i.e.* MDA-MB-231). More interestingly, we observed an ~5-fold stronger association between P(Hex-OH-AAm)-Cy5 and MCF10A. These results strongly indicate that specifically the polymeric anionic charge influences the interaction between human non-cancer cells and polyanions more drastically than that with cancer cells. The same trend – however, less pronounced – was observed for P(PhenylPr-OH-AAm)-Cy5 and P(Phe-OH-AAm)-Cy5. While zeta-potential measurements showed a comparable charge profile of these three polymers, the cell association and specificity differed. We therefore assume that in addition to the ionic charge, the aromatic side chain hinders the association with non-tumorigenic cell membranes.

2.5. Interaction of amino-acid-derived polyelectrolytes with fibroblasts

Lastly, we compared the cell association of polyelectrolytes with cancer cells to the results with fibroblasts (NIH-3T3, Fig. S20B), our previous control cell line,[53] which provides information about tissue specificity. MCF10A represented a control cell line of non-cancer breast tissue,[54,58] while NIH-3T3 and L929, both fibroblast cell lines, were chosen to represent other non-cancer cell lines which are regularly investigated in the literature and possess a cellularly excreted anionic extracellular matrix composed of hyaluronic acid, which is associated with the cells.[59]

It was observed that the overall polymer association with NIH-3T3 fibroblasts was significantly lower – except for P(Me_3Lys-OH-AAm)-Cy5, which showed higher association with the fibroblasts. An explanation for these results may be found in the extracellular matrix of fibroblasts, which is composed of a higher quantity of hyaluronic acid.[60] This polysaccharide will, as indicated by the results, repel all negatively charged polymers, while P(Me_3Lys-OH-AAm)-Cy5, which contains a permanent positive charge and thus an all-over zwitterionic charge at any physiological pH value, is able to associate due to attractive electrostatic interactions. These results highlight that polymeric interactions are strongly dependent on the cell-associated extracellular matrix. In summary, the permanently charged P(Me_3Lys-OH-AAm) exhibited the highest potential for further investigation of specific interaction with cancer cells without affecting healthy human cells of the same origin (*i.e.* breast tissue) and will be further investigated in the future.

The final part of this study focused on the clarification about the polymer uptake into cancer cells – represented by MDA-MB-231 breast cancer cells. Clarification was sought by imaging *via* confocal laser scanning microscopy (CLSM) measurements of MDA-MB-231 and L929 fibroblasts after incubation with Cy5-labelled polymers, providing information about the internalisation of the studied polyelectrolytes.

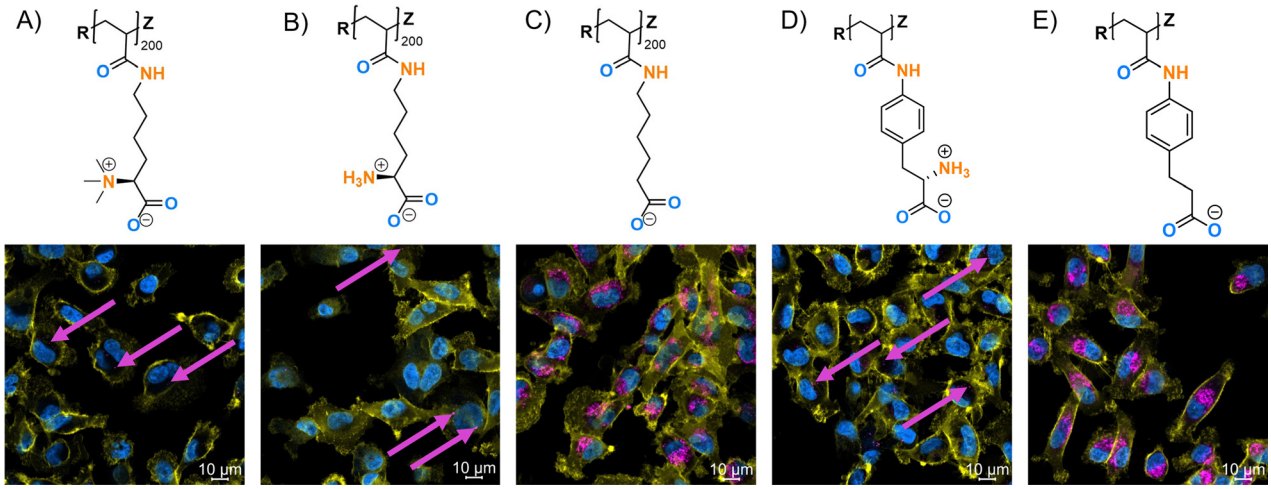

Fig. 5 MDA-MB-231 cancer cells visualised by CLSM 1 h after treatment with polymers. Blue: Hoechst 33342/nucleus. Yellow: cell membrane (CellMask™ Green Plasma Membrane stain). Magenta: Cy5/polymer channel. Cells were treated with Cy5 modified polymers (A) P(Me_3Lys-OH-AAm)-Cy5. (B) P(Lys-OH-AAm)-Cy5. (C) P(Hex-OH-AAm)-Cy5. (D) P(Phe-OH-AAm)-Cy5. (E) P(PhenylPr-OH-AAm)-Cy5.

After 1 h of incubation with MDA-MB 231, a strong intracellular fluorescence signal of the polyanions, P(Hex-OH-AAm)-Cy5 and P(PhenylPr-OH-AAm)-Cy5, was observed (Fig. 5) compared to the untreated cells (Fig. S21). It should further be noted that some clustering of fluorescence was observed, which may be derived from accumulation within the cellular ultrastructures. The results overall indicated fast and efficient polymer uptake as already suggested by flow cytometry measurements. Previously, a slow but significant accumulation of (chiral) anionic polymers in the cell membrane has been reported.[5,61,62] This is thought to be due to the combined effects of their anionic charge and hydrophobic properties, which promote membrane association and subsequent internalisation with polyanions.[5] Here, membrane accumulation appeared to be absent, suggesting that additional motifs (*e.g.* chirality) contribute to this phenomenon, which should be investigated more deeply in the future. Anionic polymers generally show limited cellular association and internalisation due to the negatively charged nature of the cell membrane surface.[36] Moreover, the rapid uptake after 1 h and the intracellular fluorescence signal even after 4 h incubation time (Fig. S21) observed for both cell lines (MDA-MB 231 and L929) and for all polyanions examined in this study, (P(Hex-OH-AAm)-Cy5 and P(PhenylPr-OH-AAm)-Cy5), highlights the significant role of hydrophobicity in promoting cell interaction and accelerating internalisation.

After 1 h incubation time, the intracellular signal of the zwitterionic polymers P(Me_3Lys-OH-AAm)-Cy5, P(Lys-OH-AAm)-Cy5 and P(Phe-OH-AAm)-Cy5 was low compared to the polyanions, revealing the lowest uptake for P(Me_3Lys-OH-AAm)-Cy5. While this was in line with the flow cytometry results of the two Lys-derived polymers, a deviation for the Phe-derived polyzwitterion was observed. Live cell imaging after 4 h incubation (Fig. S22), in turn, revealed an intracellular fluorescence signal for P(Phe-OH-AAm)-Cy5, suggesting a slower internalisation of the aromatic polyzwitterion than for the aliphatic polymers in MDA-MB 231 cells. Thus, it was demonstrated that the polymers were internalised by the cells depending on their characteristics of their side chain.

2.6. Internalisation pathways of amino-acid-derived polyelectrolytes

Several studies have reported that internalisation of macromolecules mainly follows active pathways.[63–65] Thus, we quantified the cellular internalisation of the polymers by cell incubation studies at 37 °C and 4 °C for 4 h using MDA-MB-231 breast cancer cells. A reduction in MFI measured by flow cytometry showed signals approximately 60 to 80% lower at 4 °C compared to the respective control group incubated at 37 °C (Fig. S23), indicating reduced polymer–cell interactions at decreased temperatures. At first glance, the weaker interactions at 4 °C combined with the uptake shown in Fig. 5 suggested that uptake mainly takes place *via* active transport pathways, which are often upregulated in cancer cell lines and facilitate enhanced cell growth.[66–68] However, a more detailed investigation of the complex uptake mechanism of the polymers into cells is needed since the driving force for active transport (*e.g.* ATP) requires specific inhibition to support the data. In addition, previous research by different groups has further suggested that the cell association of (amino-acid-derived) polyzwitterions is mainly driven by targeted (active) interactions with components on the cell surface of cancer cells (*i.e.* receptors or transporters) leading to an enhanced surface interaction and subsequent internalisation *via* endocytic pathways;[37] however, previous results were partly controversial, indicating an increased complexity of interactions between polyelectrolytes and cell surfaces. Based on decreased polymer–cell interaction at lower temperature,[69] the driving forces behind the cellular association of the tested amino-acid-derived polymers were investigated with respect to potential selective interactions with cell-surface transporters. Therefore, competitive inhibitors for different amino acid transporters (AATs),

which are overexpressed in MDA-MB-231 (*i.e.* SNAT1/2, ASCT1/2, LAT1/2, xCT and MCT4),[57] were applied for a short incubation time (15 min), in line with our previous study. Surprisingly, neither of the polymers showed an inhibitor-dependent decrease of uptake, as observed by constantly high MFI values (Fig. S24). These results suggested an AAT interaction-independent cell association. In general, inhibition of certain transporters can lead to overcompensation by other transporters which could interfere the tests.[70] However, additional experiments with competitive amino acids (*i.e.* leucine (Leu, main substrate of LAT transporters),[71] phenylalanine (Phe, main substrate of LAT1)[72] and glutamic acid (Glu, main substrate of xCT)[68]) for transporter interactions supported these findings (Fig. S25). Here, only leucine showed a slight trend towards a decrease of polymer cell association. These deviate from previously reported results on CT26 colon adenocarcinoma cells investigating a different kind of polyzwitterions,[37] which may be caused by the use of different cell lines.

Based on the reported results, we conclude that the studied polymers do not strongly interact with specific AATs but associate mainly *via* charge interactions with the cell membrane before active internalisation *via* endocytic pathways. Future studies will aim at examining the cellular association mechanisms with different cell lines in more detail, *e.g.* by screening a broader range of cell lines and investigating specific uptake mechanisms, aiming for a better understanding of uptake and distribution of polymers inside the cell.

3. Conclusions

The synthesis of amino-acid-derived polyelectrolytes from lysine- and phenylalanine-derived motifs by PPM polymerisation was demonstrated. Defined polyzwitterions were prepared by using Boc-protected compounds and subsequent deprotection. Anionic structural analogues were synthesised likewise. *Via* this approach a library of five polymers were obtained, which enabled a study of the effects of side chain alterations on the properties of amino-acid-derived polyelectrolytes. We investigated the influence of a (permanent) zwitterionic character compared to anionic motifs and, additionally, the influence of aliphatic and aromatic side chain spacers on both the physicochemical and the biological properties/behaviour. HPLC showed that aromaticity in the side chain increased the hydrophobicity, at pH $\approx$ 2, for anionic polymers while no influence was observed for the zwitterionic analogues. pH-dependent DLS measurements were performed. Here aggregation around and below the pK_a was observed for the anionic polymers. Smaller aggregates were formed around the pI with both zwitterionic polymers P(Me_3Lys-OH-AAm) and P(Phe-OH-AAm), between pH 6 and 7, which can enhance retention within tumour tissue as the external pH at tumour sites is slightly lower. Furthermore, DLS measurements in combination with model proteins showed no aggregation with most polymers. Interestingly, the more hydrophobic aromatic anionic polymer, formed larger aggregates, whereas the less hydrophobic aliphatic polymer did not aggregate. The polymers showed no aggregation in the presence of FBS, allowing further cell experiments. Here, all synthesised polymers were well tolerated by MDA-MB-231 breast cancer cells at concentrations up to 1 mg mL^{-1} (for 24 h). Cell association with different cell lines showed higher interaction with tumorigenic cells. Further experiments, to understand the uptake mechanism were performed by specific amino acid transporter inhibition and competitive uptake assays which revealed no dependence on the studied transporters; however, a strong energy-dependent uptake was observed based on the presented results. The fast cellular uptake of the anionic polymers, which was observed by CLSM measurements, makes them interesting candidates for further studies towards drug-delivery applications.

4. Experimental part

4.1. Materials and instrumentation

4.1.1. Materials. Acetonitrile (99.9%), diethyl ether (99.5%), dimethylformamide (99.5%), methanol (99.9%) and sodium hydrogen carbonate (>99.7%) were purchased from FisherScientific. Chloroform (99.8%), dichloromethane (99.8%), isopropanol (99.9%), sodium hydroxide (99.5%), potassium hydroxide (99.5%), hydrochloric acid (32%), Dulbecco's PBS (DPBS), bovine serum albumin (BSA) and lysozyme, from which the last two obtained as lyophilised powders, were purchased from VWR Chemicals. Triethylamine (99.5%), 4-(4,6-dimethoxy-1,3,5-triazin-2-yl)-4-methylmorpholiniumtetrafluorborat (DMTMM·BF_4, 97%) and potassium carbonate (99.0%) were purchased from Sigma Aldrich. Cyanine5-amine (95.0%) was purchased from Lumiprobe. 3-(4-Aminophenyl)propanoic acid (98%), *N*-hydroxysuccinimide (98.0%), 2-amino-2-norbornanecarboxylic acid (BCH, 95%), *O*-benzyl-L-serine (BzlSer, 98%), sulfasalazine (98%), 5-((5-chloro-2-((5-ethoxyquinoline)-8-sulfonamido)phenyl)ethynyl)-4-methoxypicolinic acid (MSC-4381, 98%) and *N*-(*tert*-butoxycarbonyl)-4-amino-L-phenylalanine (98%) were purchased from BLD Pharmatech Ltd. Trifluoroacetic acid (99.0%) was purchased from abcr. Acryloyl chloride (96%) and dilauryl peroxide (Luperox, 97%) were purchased from ThermoScientific. Boc-Lys-OH (98%) was purchased from Carbolution. 6-Aminohexanoic acid (6-AmHex-OH, >98.5%) was purchased from Fluka.

Azobis(isobutyronitrile) (AIBN) (Fluka or Sigma Aldrich, 98.0%) was recrystallized from methanol before use. *N*-Acryloxysuccinimide (NAS)[73] and 2-(((butylthio)carbonothioyl)thio)propanoic acid (PABTC)[74] were synthesised and characterised following known procedures in the literature.

RPMI 1640 medium (Sigma Aldrich), Dulbecco's Modified Eagle's Medium low glucose (Sigma Aldrich), Dulbecco's Modified Eagle's Medium (DMEM/F12; Sigma Aldrich), DMEM-LPSTA (Capricorn), Mammary Epithelial Cell Basal Medium (PromoCell) supplemented with BPE-26, hEGF-5, Insulin-2.5, and HC-250, foetal bovine serum (FBS; Bio&Sell), penicillin/streptomycin (Bio&Sell), Dulbecco's 1× PBS (Capricorn), choleratoxin (Sigma Aldrich), NIH-3T3 (ACC 59, DSMZ), MDA-MB 231 (HTB-26, ATCC), HCC-78 (ACC 563, DSMZ), MCF10A (#305026, Cytion), L929 (#400260, CLS), DMEM-LPSTA (Capricorn), MDA-MB-231

ACC-732 (DSMZ), CellMask™ Plasma Membrane Stain Green (Thermo Fisher Scientific), Hoechst33342, trihydrochloride, trihydrate (Thermo Fisher Scientific), 4% paraformaldehyde solution in DPBS (Thermo Fisher Scientific), µ-plate 24 well (IBIDI), µ-plate 96 well square (IBIDI), and IBIDI anti-evaporation oil (IBIDI) were used.

4.1.2. Proton nuclear resonance (^{1}H NMR) spectroscopy. ^{1}H NMR spectra were recorded on a Bruker Avance 300 (300 MHz) spectrometer equipped with a BACS-120 autosampler and a ^{1}H, ^{13}C, ^{19}F and ^{31}P-BBO probe at room temperature.

4.1.3. Size-exclusion chromatography (SEC). Aqueous SEC measurements of P(Boc-Lys-OH-AAm), P(Lys-OH-AAm), P(Hex-OH-AAm), P(Boc-Phe-OH-AAm), P(Phe-OH-AAm), P(PhenylPr-OH-AAm), P(Boc-Lys-OH-AAm)-Cy5, P(Lys-OH-AAm)-Cy5, P(Me$_3$Lys-OH-AAm)-Cy5, P(Hex-OH-AAm)-Cy5, P(Boc-Phe-OH-AAm)-Cy5, P(Phe-OH-AAm)-Cy5 and P(PhenylPr-OH-AAm)-Cy5 were performed on an instrument consisting of a column set with a Suprema precolumn (particle size = 5 µm) and three Suprema main columns (particle size = 5 µm, 1 × 30 Å; 2 × 1000 Å) with a separation range from 100 to 1 000 000 Da (PSS) together with a variable wavelength detector (1200 Series, Agilent Technologies). As solvent 0.07 M aqueous Na_2HPO_4 was used (for dissolving the polymer and as eluting solvent) with a flow rate of 0.8 mL min^{-1} and the columns were maintained at room temperature. As the internal standard, ethylene glycol (HPLC grade) was used. The calibration was done with narrowly distributed poly(methacrylic acid) sodium salt homopolymers (PMA Na salt; PSS calibration kit). An injection volume of 60 µL was used for the measurements. The samples were concentrated to 2 mg mL^{-1} and filtered through a 0.22 µm nylon filter before analysis. The UV-detector was set to λ = 600 nm for measurements of Cy5-labeled polymers.

Reported molar masses of polymers in this study are based on the indicated standards and denoted as $M_{n,app}$.

Aqueous SEC measurements of P(Me$_3$Lys-OMe-AAm) and P(Me$_3$Lys-OMe-AAm)-Cy5 were performed on an instrument consisting of a column set with a NOVEMA Max precolumn (particle size = 10 µm) and three NOVEMA Max main columns (particle size = 10 µm, 1 × 100 Å; 2 × 3000 Å) with the separation range from 100 to 3 000 000 Da (PSS, Mainz, Germany) together with a variable wavelength detector (1200 Series, Agilent Technologies). As solvent 80 : 20 water/ACN mixture + 0.1 M NaCl + 0.1 V% TFA was used (for dissolving the polymer and as eluting solvent) with a flow rate of 0.8 mL min^{-1} and columns maintained at room temperature. As the internal standard ethylene glycol (HPLC grade) was used. The calibration was done with narrowly distributed poly(2-vinylpyridine) (narrowly distributed P2VP homopolymers, PSS calibration kit). An injection volume of 60 µL was used for the measurements. The samples were concentrated to 2 mg mL^{-1} and filtered through a 0.22 µm nylon filter before analysis. The UV-detector was set to λ = 600 nm for measurements of Cy5-labeled polymers.

Size-exclusion chromatography of PNAS and PNAM was performed on an Agilent 1260 Infinity II system equipped with the MDS refractive index detector, MWD (UV), MDS viscometer, PSS SLD 7100 multi-angle light scattering detector and PSS GRAM 30 and 1000 column sets with DMAc (+5 g L^{-1} LiBr) as the eluent. Measurements were conducted with 100 µL injection volume at a constant flow rate of 1 mL min^{-1}, with the column oven held at 40 °C. All samples were filtered (PTFE 0.22 µm) before the measurement. For calibration, narrowly distributed poly(ethylene oxide) (PEO) standards were used. The UV-detector was set to λ = 600 nm for measurements of Cy5-labeled polymers and λ = 310 nm for end-group removal.

Table 2 Composition of the HPLC eluent at indicated time points

Time [min]	Fraction of 0.1 v/v% aqueous TFA [%]	Fraction of acetonitrile [%]
0	98.0	2.0
5	50.0	50.0
10	0.0	100.0
17	0.0	100.0
25	98.0	2.0
35	98.0	2.0

4.1.4. High-performance liquid chromatography (HPLC). HPLC measurements were conducted with a Jupiter 5 µm C18 300 Å LC column (250 × 4.6 mm). The run time was 35 min. A mixture of 0.1 v/v% TFA in water and acetonitrile served as the eluent (Table 2). The fluorescence detection was set to λ_{ex} = 640 nm and λ_{em} = 680 nm with 1× gain. The ELSD detector was set to λ = 215 nm.

4.1.5. Data analysis of theoretical log *P* values. To obtain the theoretical partition coefficients (log *P* values), the cheminformatics tool RDkit with the descriptor Mollog *P* (based on Wildman and Crippen)[44,52] was used. The calculation was done for one repeating unit of each polymer. For this purpose, the following Simplified Molecular Input Line Entry System (SMILES) strings were used:

P(PhenylPr-OH-AAm): C(C)CC(=O)Nc1ccc(CCC(=O)O)cc1

P(Phe-OH-AAm):
C(C)CC(=O)Nc1ccc(CC([NH$_3^+$])C(=O)O)cc1

P(Hex-OH-AAm): C(C)CC(=O)NCCCCCCC(=O)O

P(Me$_3$Lys-OH-AAm):
C(C)CC(=O)NCCCCC(C(=O)O)[N$^+$](C)(C)C

P(Lys-OH-AAm): C(C)CC(=O)NCCCCC([NH$_3^+$])C(=O)O

4.1.6. Theoretical ionisation state and polymer net charge. The theoretical ionisation state of each pH responsive group in the polymers was calculated *via* the Henderson Hasselbalch equation (eqn (1)).

$$\text{Deprotonated fraction (\%)} = \frac{1}{1 + 10^{pK_a - pH}} \times 100\% \quad (1)$$

For calculations the following pK_a values were used as approximation:

P(Lys-OH-AAm): 2.17 (COOH, lysine), 9.13 (α-NH$_2$, lysine)[75]

P(Me$_3$Lys-OH-AAm): 1.84 (COOH, betaine)[76]

P(Hex-OH-AAm): 4.88 (COOH, hexanoic acid)[77]

P(Phe-OH-AAm): 1.83 (COOH, phenylalanine), 9.13 (NH$_2$, phenylalanine)[78]

P(PhenylPr-OH-AAm): 4.73 (COOH, phenylpropionic acid)[75]

The polymer net charge was derived from the proportion of anionic and cationic moieties in the charged state, respectively.

4.1.7. Dynamic light scattering (DLS). DLS was measured on a Malvern Panalytical Zetasizer Ultra device using disposable folded capillary cuvettes. The excitation light source was a He–Ne laser at 633 nm and the intensity of the scattered light was measured at an angle of 173°. The light scattering was measured during an automatic measurement process from minimum 15 runs of 1.68 s run duration or 30 runs of 1.68 s each for each sample. Measurement parameters were set to an equilibrium time and temperature of 60 s and 37 °C. This method measures the rate of intensity fluctuation, and the size of the particles is determined through the Stokes–Einstein equation. The concentration of the polymer solution was 2 mg mL^{-1}. For the pH-responsive measurements, a 2 mg mL^{-1} solution of the polymer in deionised water was prepared and 0.1 M aq. NaOH or aq. HCl were added until the desired pH-value was reached. Measurements were done with a Mettler Toledo digital pH meter.

4.1.8. Electrophoretic light scattering (ELS). ELS was used to measure the zeta potential (ζ). The measurement was also performed on a Malvern Panalytical Zetasizer ultra device using 1.5 mL semi-micro cuvettes or disposable folded capillary cuvettes by applying laser Doppler velocimetry. For each measurement, automatic measurements including min. 10 runs were carried out using the slow-field reversal and the fast-field reversal mode at 150 V. Each experiment was performed in triplicate at 37 °C after an equilibration time of 60 s. The zeta potential was calculated from the electrophoretic mobility (μ) according to the Henry equation. The Henry coefficient $f(k_a)$ was calculated according to Ohshima.[79] The polymer solutions were similarly prepared as for during the DLS measurements.

4.2. Synthesis and characterization

4.2.1. Poly(*N*-acryloyl succinimide) (PNAS). 2 g of NAS (12 mmol, 200 equiv.) were transferred into a microwave tube (Biotage) equipped with a stirring bar. 0.984 mg (0.006 mmol, 0.1 equiv.) of AIBN and 14.28 mg (0.06 mmol, 1 equiv.) of PABTC were added, using stock solutions in DMF, followed by addition of DMF to reach a final volume of 4 mL. The tube was closed with a septum and vortexed until homogeneous before a sample was taken (t = 0 h) for ^{1}H-NMR spectroscopy in DMSO-d6 to determine the conversion by comparing the sample with a sample at the end of the reaction. The reaction mixture was deoxygenated by putting the mixture under an argon flow for 30 min and afterwards the tube was placed in a preheated oil bath and stirred at 70 °C for 24 h. The reaction was terminated by cooling to RT and purging in air. A sample was taken and analysed *via* ^{1}H-NMR spectroscopy in DMSO-d6. The crude polymer was precipitated in diethyl ether (−80 °C) twice. After centrifugation (5000 rpm, 5 min.), the supernatant was discarded, and the polymer was dried under reduced pressure overnight to obtain the product as a yellow viscous oil.

The X_n of the resulting polymer was calculated from ^{1}H NMR (Fig. S26) by using the signal of the vinyl CH_2-group at δ = 6.35 ppm and the reaction solvent at δ = 7.96 ppm both at t = 0 h and 24 h. The reaction solvent was used as an internal standard and the decrease of the vinyl signal in relation to the standard was calculated, providing information about the monomer conversion. The conversion was then multiplied with the initial [M]/[CTA] ratio to obtain the average degree of polymerisation, *i.e.* an X_n of 188 for P(Me_3Lys-OH-AAm) and 193 for all others.

Table 3 Quantities of reagents used for the PPM of PNAS

Amino acid	n [mmol]	m [mg]
Boc-Lys-OH	1.2	297
Me_3Lys-OMe-NH_2	1.2	263
6-AmHex-OH	1.2	158
Boc-4-AmPhe-OH	1.2	337
4-AmPhenylPr-OH	1.2	199

Polymers were analysed by DMAc SEC (Fig. S27, standard: PEG).

PNAS for P(Me_3Lys-OH-AAm): $M_{n,app}$ = 4700 g mol^{-1}; $Đ$ = 1.84

PNAS for all others: $M_{n,app}$ = 8100 g mol^{-1}; $Đ$ = 1.87

4.2.2. Post-polymerisation modification of PNAS with Boc-Lys-OH, Me_3Lys-OMe-NH_2, 6-AmHex-OH, Boc-4-AmPhe-OH, and 4-AmPhenylPr-OH. The post-polymerisation modification of PNAS is exemplary described for reactions with Boc-Lys-OH yielding P(Boc-Lys-OH-AAm). Quantities and moles are given relative to the single repeating unit NAS of the polymer and can be found in Table 3.

In a 20 mL reaction vessel (Biotage), PNAS (200 mg, 0.6 mmol, 1.00 equiv.) was dissolved in anhydrous DMF (9.5 mL). 500 µL of triethylamine were added. Afterwards, Boc-Lys-OH (297 mg, 1.2 mmol, 1.03 equiv.) was added, the reaction vial was closed with a septum, and the suspension was stirred at RT for 24 h. Then, the product was purified by dialysis (RC, MWCO 3.5 kDa, SpectraPor) against 1 L brine for one day followed by dialysis against 1 L of deionised water for three days with daily water change. Upon lyophilisation, the product was obtained as an off-white powder. Polymers were analysed *via* ^{1}H NMR and aqueous SEC.

Polymers were analysed by aqueous SEC (0.07 M aq. Na_2HPO_4 (standard: PMA Na salt)). Elugrams can be found in Fig. S6.

P(Boc-Lys-OH-AAm): $M_{n,app}$ = 17 200 g mol^{-1}; $Đ$ = 2.25.

P(Hex-OH-AAm): $M_{n,app}$ = 16 500 g mol^{-1}; $Đ$ = 2.30.

P(Boc-Phe-OH-AAm): $M_{n,app}$ = 12 800 g mol^{-1}; $Đ$ = 2.48.

P(PhenylPr -OH-AAm): $M_{n,app}$ = 11 000 g mol^{-1}; $Đ$ = 2.71.

4.2.3. Post-polymerisation modification of PNAS with Cy5-amine, Boc-Lys-OH, Me_3Lys-OMe-NH_2, 6-AmHex-OH, Boc-4-AmPhe-OH, and 4-AmPhenylPr-OH. The post-polymerisation modification of PNAS is exemplary described for reactions with Boc-Lys-OH yielding P(Boc-Lys-OH-AAm)-Cy5. Quantities and moles are given relative to the single repeating unit NAS of the polymer and can be found in Table 4.

In a 5 mL reaction vessel (Biotage), PNAS (49 mg, 1.4 µmol, 1.00 equiv.) was dissolved in anhydrous DMF (900 µL). 1 mg of Cy5-amine (1.5 µmol, 1.1 equiv.) was added. Afterwards, 8 µL of a 1 : 10 [triethylamine/DMF] mixture were added, and the reaction vessel was closed with a septum. The reaction mixture was stirred in the dark at RT for 24 h. Then, 53 µL of triethylamine and Boc-Lys-OH (73 mg, 0.3 mmol, 1.03 equiv.) as well as 940 µL

Table 4 Quantities of reagents used for the PPM of PNAS

Amino acid	n [mmol]	m [mg]
Boc-Lys-OH	0.3	73
Me_3Lys-OMe-NH_2		68
6-AmHex-OH		39
Boc-4-AmPhe-OH		83
4-AmPhenylPr-OH		48.7

DMF were added. The reaction vial was closed with a septum, and the suspension was stirred at RT for 24 h. Then, the product was purified by dialysis (RC, MWCO 3.5 kDa, SpectraPor) against 1 L brine for one day followed 1 L deionised water for three days with daily water change. Upon lyophilisation, the product was obtained as a blue powder.

Polymers were analysed by aqueous SEC (0.07 M aq. Na_2HPO_4 (standard: PMA Na salt)).

P(Boc-Lys-OH-AAm)-Cy5: $M_{n,app}$ = 18 600 g mol^{-1}; $Đ$ = 2.02.

P(Hex-OH-AAm)-Cy5: $M_{n,app}$ = 15 900 g mol^{-1}; $Đ$ = 2.26.

P(Boc-Phe-OH-AAm)-Cy5: $M_{n,app}$ = 14 800 g mol^{-1}; $Đ$ = 2.47.

P(PhenylPr -OH-AAm)-Cy5: $M_{n,app}$ = 15 700 g mol^{-1}; $Đ$ = 2.54.

4.2.4. Acidic deprotection of P(Boc-Lys-AAm) and P(Boc-Phe-AAm) yielding P(Lys-AAm) and P(Phe-AAm), respectively. 100 mg P(Boc-Lys-AAm) and P(Boc-Phe-AAm) were stirred in a 10 mL 50/50 V% [TFA : water] mixture overnight. 30 mg P(Boc-Lys-AAm)-Cy5 and P(Boc-Phe-AAm)-Cy5 were stirred in the dark in a 4 mL 50/50 V% [TFA : water] mixture overnight. Subsequently, the reaction mixture was purified by dialysis (RC, MWCO 3.5 kDa, SpectraPor) against 1 L of deionised water for one day with one water change after five hours followed by lyophilisation to obtain P(Lys-AAm), P(Phe-AAm), P(Lys-AAm)-Cy5 and P(Phe-AAm)-Cy5.

Polymers were analysed by aqueous SEC (0.07 M aq. Na_2HPO_4 (standard: PMA Na salt)).

P(Lys-OH-AAm): $M_{n,app}$ = 2000 g mol^{-1}; $Đ$ = 3.27.

P(Phe-OH-AAm): $M_{n,app}$ = 13 000 g mol^{-1}; $Đ$ = 2.14.

P(Lys-OH-AAm)-Cy5: $M_{n,app}$ = 4700 g mol^{-1}; $Đ$ = 2.08.

P(Phe-OH-AAm)-Cy5: $M_{n,app}$ = 12 000 g mol^{-1}; $Đ$ = 2.59.

4.2.5. Poly(*N*-acyrloylmorpholine) (PNAM). 1.78 mL of NAM (2 g, 14.2 mmol, 200 equiv.) were transferred into a microwave tube (Biotage) equipped with a stirring bar. 1.163 mg (0.0071 mmol, 0.1 equiv.) of AIBN and 16.887 mg (0.071 mmol, 1 equiv.) of PABTC were added, using stock solutions, followed by addition of DMF to reach a final volume of 4 mL. The tube was closed with a septum and vortexed until homogeneous before a sample was taken (t = 0 h) for ^{1}H-NMR spectroscopy in DMSO-d6 to determine the conversion by comparing the sample with a sample at the end of the reaction. The reaction mixture was deoxygenated by putting the mixture under an argon flow for 30 min and afterwards the tube was placed in a preheated oil bath and stirred at 70 °C for 24 h. The reaction was terminated by cooling to RT and purging in air. A sample was taken and analysed *via* ^{1}H-NMR spectroscopy in DMSO-d6. The crude polymer was precipitated in diethyl ether (−80 °C). After centrifugation (5000 rpm, 5 min.), the supernatant was discarded, and the polymer was dried under reduced pressure overnight to obtain the product as a yellow viscous oil.

The X_n of the resulting polymer was calculated by using the signal of the vinyl CH_2-group at δ = 5.70 ppm and the reaction solvent at δ = 2.90 ppm both at t = 0 h and 24 h, resulting in a X_n of 198.

The polymer was analysed by DMAc SEC (Fig. S28; standard: PEG).

PNAM-CTA: $M_{n,app}$ = 8300 g mol^{-1}; $Đ$ = 1.48.

4.2.6. CTA removal of PNAM. The end-group removal of trithiocarbonates was conducted according to a literature procedure.[80]

In a reaction vessel equipped with a stirrer bar, 1.5 g of P(NAM)-CTA (52.5 × 10^{-6} mol, 1.0 equiv), 173.02 mg of AIBN (1.05 mmol, 20.0 equiv), and 42 mg of Luperox (0.11 mmol, 2.0 equiv) were dissolved in 15 mL of toluene. The vessel was sealed with a septum, and the reaction mixture was deoxygenated with argon for 30 min. Subsequently, the vial was placed in a preheated oil bath and heated to 80 °C for 2 h under continuous stirring. After cooling to RT, the crude mixture was precipitated in diethyl ether. After centrifugation (5000 rpm, 5 min.), the supernatant was discarded, and the polymer was dried under reduced pressure overnight to obtain the product as a transparent viscous oil. Complete removal of the trithiocarbonate end group was analysed by SEC measurements in DMAc using a UV detector (λ = 310 nm), showing the disappearance of the polymer UV trace (Fig. S28).

PNAM-EGR: $M_{n,app}$ = 1300 g mol^{-1}; $Đ$ = 1.77.

4.2.7. Cy5-labelling of PNAM-EGR. In a small reaction vessel, 50 mg of PNAM-EGR (16.0 × 10^{-6} mol, 1.0 equiv.) and 14.47 mg of DMTMM·BF_4 (0.04 mmol, 2.5 equiv.) were dissolved in 20 mL of anhydrous DMF and stirred at RT for 30 min. Subsequently, a 10 mg mL^{-1} solution of Cy5-amine (34.6 mg, 0.05 mol, 3.0 equiv.) in anhydrous DMF was added. The reaction was stirred at RT in the dark overnight. Then, the reaction mixture was precipitated in diethyl ether. After centrifugation (5000 rpm, 5 min), the supernatant was discarded. The crude product was redissolved in water. Then, the product was purified by dialysis (RC, MWCO 3.5 kDa, SpectraPor) against 1 L of brine for one day followed by dialysis against 1 L of deionised water for three days with daily water change. Upon lyophilisation, the product was obtained as a blue powder. Dye attachment and purity from unattached dye were confirmed by SEC (Fig. S28; λ = 612 nm).

The polymer was analysed by DMAc SEC (standard: PEG).

PNAM-Cy5: $M_{n,app}$ = 18 900 g mol^{-1}; $Đ$ = 1.31.

4.3. Biological evaluation

4.3.1. Protein fouling. Aggregation of P(Lys-OH-AAm), P(Me_3Lys-OH-AAm), P(Hex-OH-AAm), P(Phe-OH-AAm) and P(PhenylPr-OH-AAm) after incubation with dedicated proteins (BSA and lysozyme) was analysed by DLS measurements. Stock solutions of the polymers and the proteins were prepared separately in DPBS (1 mg mL^{-1}) and mixed in a ratio of 1 : 1, resulting in final concentrations of c = 0.5 mg mL^{-1}. The samples were analysed immediately after mixing (t = 0 h) and at indicated time points (0.5 h, 1 h, 2 h, 4 h, 24 h) thereafter. In between measurements, the samples were incubated at

37 °C whilst being shaken at 100 rpm on a thermostated shaker. Measurements were conducted at 37 °C with five measurements and three runs each. After the measurement, samples were placed back into the thermostated shaker immediately.

4.3.2. Polymer stability towards FBS-containing DPBS. Aggregation of P(Lys-OH-AAm), P(Me_3Lys-OH-AAm), P(Hex-OH-AAm), P(Phe-OH-AAm) and P(PhenylPr-OH-AAm) after incubation in DPBS solution containing 10 V% FBS was analysed by DLS measurements. Polymers were weighed in and dissolved into the mixture to obtain a final concentration of c = 0.1 mg mL^{-1}. The samples were analysed immediately after mixing (t = 0 h) and at indicated time points (0 h, 5 min, 10 min, 0.5 h, 1 h, 2 h and 5 h) thereafter. In between measurements, the samples were incubated at 37 °C without shaking. The light scattering was measured during 30 runs of 1.68 s each for each sample. Measurement parameters were set to an equilibrium time and temperature of 60 s and 37 °C.

4.3.3. Cell culture. MDA-MB-231 cells (HTB-26, ATCC) were maintained in DMEM/F12 cell culture medium, HCC-78 cells were cultured in RPMI 1640 medium, and NIH-3T3 and L929 were cultured in Dulbecco's Modified Eagle's Medium low glucose. All those media were supplemented with 10% foetal bovine serum (FBS), 100 μg mL^{-1} streptomycin, and 100 U mL^{-1} penicillin each. MCF10A cells were maintained in Mammary Epithelial Cell Growth Medium with supplements and 100 ng mL^{-1} choleratoxin. All cells were cultivated at 37 °C in a humidified 5% CO_2 atmosphere.

4.3.4. Cell viability assay. The cell viability assay was slightly modified from our previous procedure.[42] The cytotoxicity of P(Lys-OH-AAm), P(Me_3Lys-OH-AAm), P(Hex-OH-AAm), P(Phe-OH-AAm) and P(PhenylPr-OH-AAm) was tested using MDA-MB-231 breast cancer cells. The polymers stock solutions were prepared at concentrations ≤ 20 mg mL^{-1} in demineralised water. The polymers were tested in a concentration range from 0 to 1.0 mg mL^{-1}. MDA-MB-231 cells were cultured as described above. For the cell viability assay, cells (10^4 per well) were seeded in 96-well plates and allowed to adhere overnight. No cells were seeded in the outer wells. The medium was subsequently removed and replaced by fresh polymer containing media. Then, the cells were incubated at 37 °C for an additional 24 h. After that, the medium was removed, the cells were washed with 100 μL DPBS per well, and then fresh medium containing thiazolyl blue tetrazolium bromide (MTT) (concentration: 1 mg mL^{-1}) was added (100 μL per well). Note: MTT (50 mg) was dissolved in 10 mL of sterile DPBS, filtered (membrane, 0.22 μm), and 1 to 5 diluted in culture medium prior to use in this assay. After incubation for 3 h at 37 °C, the test medium was discarded, 100 μL per well of *i*PrOH was added to each well and the plates were gently shaken in the dark for 15 min to dissolve the formazan crystals. Quantification was done by measuring the absorbance at λ = 580 nm using a microplate reader (Genios Pro, Tecan). Untreated cells on the same plate served as a negative control (100% viability), cells treated with 20% DMSO as a positive control (0% viability), and wells without cells as background. Experiments were performed in triplicate on three different plates. Relative cell viability was calculated by using eqn (2).

$$\%\,\text{Cell viability} = \frac{\text{Abs. sample} - \text{Abs. background}}{\text{Abs. negative control} - \text{Abs. background}} \times 100 \quad (2)$$

4.3.5. Cell association analysis *via* flow cytometry

4.3.5.1. Cell association assay I: concentration-dependent polymer association with cells. The MDA-MB-231 cells were cultured as described above. For the experiments, 2 × 10^5 cells mL^{-1} were seeded in 2 mL of culture medium in a 6 well plate and cultivated for 24 h prior to treatment. 90 minutes before treatment, the medium was changed to 900 μL of fresh culture medium. The polymers were diluted in DPBS to a concentration of c = 0.2, 1, 5 and 25 μM and added to the wells (100 μL). The corresponding final concentrations of each polymer were c = 0.04, 0.2, 1.0 and 2.5 μM. As a negative control (NC), cells were incubated with 100 μL DPBS. After 90 minutes of incubation at 37 °C in the cell culture incubator, the supernatant was discarded. After a washing step with DPBS cells were harvested by trypsinization, followed by centrifugation and resuspension in DPBS. Flow cytometry measurements were performed using a CytoFLEX S flow cytometer (Beckman Coulter, Krefeld, Germany) equipped with 405 nm, 488 nm and 561 nm lasers. Forward scatter (FSC), side scatter (SSC), Cy5 fluorescence (PC7 filter, 780/760 nm), and propidium iodide (PI) fluorescence (emission 620 nm) were recorded. Negative control samples (mock-treated cells) were used to set measurement parameters and define background fluorescence levels. For each sample, data from at least 10,000 events were collected. Cells were first gated based on FSC and SSC signals (linear scale) to select the non-apoptotic cell population and exclude debris and aggregates (Gate: ''Cells''). Subsequently, FSC-A *versus* FSC-H gating (linear scale) was applied to exclude doublets (Gate: ''Single cells''). The relative Cy5 fluorescence of the gated single-cell population was then quantified, enabling statistical analysis of Cy5-labelled polymer–cell interactions. Cy5-positive cells were defined as those exhibiting fluorescence intensities exceeding the autofluorescence of the negative control cells. In parallel, PI fluorescence was used to assess cell viability. Fluorescence intensity histograms (logarithmic scale) were analysed to quantify polymer–cell interactions, expressed as the mean fluorescence intensity (MFI). A detailed gating strategy is provided in Fig. S29.

The mean fluorescence intensity (MFI) was normalised to the negative control using eqn (3).

$$\text{Normalized MFI [a.u.]} = \frac{\text{MFI}_{\text{sample}}}{\text{MFI}_{\text{NC}}} \times \frac{1}{\text{fluorescence}_{\text{sample}}} \quad (3)$$

4.3.5.2. Cell association assay II: time- and temperature-dependent polymer association with cells. The cell association assay was adapted from Leiske *et al.*[6] Polymers were investigated for their association with MDA-MB-231, NIH-3T3, HCC-78 and MCF10a. In detail, 4 × 10^5 MDA-MB-231 cells per well were

seeded in a 6-well plate while 2×10^5 HCC-78 cells, 1.8×10^5 NIH-3T3 cells and 4×10^5 MCF10A cells per well were seeded in a 24-well plate and cultivated for 24 h. Then, the media were substituted with 450 μL per well fresh medium. After dilution of the polymers in DPBS to a concentration of c = 25 μM, 50 μL per well of the respective polymer was added and incubated for 4.0 h at 37 °C and in the cell culture incubator (final c = 2.5 μM). The NC contained only 50 μL of DPBS. Moreover, an additional 6-well plate with MDA-MB-231 cells was treated identically, albeit for 4 h at 4 °C (refrigerator). After 4 h of incubation at 37 °C and in the cell culture incubator or 4 °C, the cells were collected for flow cytometer measurements as described above (see Cell association assay I) (n = 4 (two duplicates)). A detailed gating strategy is provided in Fig. S30–S33.

The MFI was normalised to MFI of PNAM-treated cells using eqn (4).

$$\text{Normalised MFI [a.u.]} = \frac{\left(\frac{\text{MFI}_{\text{sample}}}{\text{MFI}_{\text{NC}}} \times \frac{1}{\text{fluorescence}_{\text{sample}}}\right)}{\left(\frac{\text{MFI}_{\text{PNAM}}}{\text{MFI}_{\text{NC}}} \times \frac{1}{\text{fluorescence}_{\text{PNAM}}}\right)} \quad (4)$$

Association relative to MCF10A using eqn (5)

$$\text{Association relative to MCF10A [\%]} = \left(\frac{\text{Normalised MFI}}{\text{Normalised MFI MCF10A}}\right) \times 100 \quad (5)$$

The temperature-dependent reduction of cell association was calculated using eqn (6).

$$\text{Relative cell association} = \frac{\text{MFI}_{4^\circ\text{C}}(\text{normalized})}{\text{MFI}_{37^\circ\text{C}}(\text{normalized})} \quad (6)$$

4.3.5.3. Cell association assay III: polymer–cell association by blocking amino-acid transporters and competitive uptake. 2×10^5 MDA-MB-231 cells per well were seeded in a 24-well plate and cultivated for 24 h. Afterward, the medium was replaced by fresh medium without FBS (225 μL per well). For the blocking of transporters, selected amino-acid transporter inhibitors were dissolved in DPBS with final concentrations of 100 mM (BzlSer), 100 mM (BCH), 1 mM (Sulfasalazine), and 0.5 μM (MSC-4381) and added to the wells (25 μL per well). The inhibitor selectivity profile is provided in Table 5. After 15 min of incubation, the medium was discarded and the cells were washed with DPBS. Fresh medium was added (450 μL per well) and the prepared polymer solutions in DPBS (c = 25 μM) were added (50 μL per well).

For assays with competitive amino acids, a 10× stock of the corresponding compound was prepared in DPBS and then mixed with cell culture media to obtain the 1× concentration. Then, the media were substituted with 450 μL per well fresh medium containing the competing amino acids. After dilution of the polymers in DPBS to a concentration of c = 25 μM, 50 μL per well of the respective polymer was added and incubated for 4 h at 37 °C in the cell culture incubator (final c = 2.5 μM). The NC contained only 50 μL of DPBS. After an incubation time of 4 h at 37 °C in the cell culture incubator, the cells were collected for flow cytometer measurements as described above (see cell association assay I) (n = 2 + 2 in the AAT blocking experiment and n = 2 in the competitive uptake experiment). A detailed gating strategy is provided in Fig. S34. The normalised MFI was calculated using eqn (3). The inhibitor-dependent reduction of cell association was calculated using eqn (7).

$$\text{Relative cell association} = \frac{\text{MFI}_{\text{without inhibitor}}(\text{normalized})}{\text{MFI}_{\text{with inhibitor}}(\text{normalized})} \quad (7)$$

Table 5 Inhibitor selectivity profile across amino acid and monocarboxylate transporters. Alanine/Serine/Cysteine Transporter 1 (ASCT1), Alanine/Serine/Cysteine Transporter 2 (ASCT2), L-type Amino Acid Transporter 1 (LAT1), L-type Amino Acid Transporter 2 (LAT2), Sodium-coupled Neutral Amino Acid Transporter 1 (SNAT1), Sodium-coupled Neutral Amino Acid Transporter 2 (SNAT2), Cystine/Glutamate Antiporter light chain (xCT; system xc^-), and Monocarboxylate Transporter 4 (MCT4). "Yes" indicates reported inhibition/interaction in this dataset; "No" indicates no reports on activity. Activities reported according to the vendor

Inhibitor	ASCT1	ASCT2	LAT1	LAT2	SNAT1	SNAT2	xCT	MCT4
BzlSer	Yes	Yes	Yes	No	Yes	Yes	No	No
BCH	No	No	Yes	Yes	No	No	No	No
MSC-4381	No	No	No	No	No	No	No	Yes
Sulfasalazine	No	No	No	No	No	No	Yes	No

4.3.6. Confocal microscopy. For confocal laser scanning microscopy (CLSM), MDA-MB231 cells (DSMZ, ACC 732) were seeded with 2×10^5 cells mL^{-1} and cultured at 37 °C in a humidified 5% v/v CO_2 atmosphere in Dulbecco's modified Eagle medium (DMEM) low glucose (1 g L^{-1}). The medium was supplemented with 10% v/v foetal bovine serum (FBS), 100 U mL^{-1} penicillin and 100 μg mL^{-1} streptomycin (culture medium). For the experiments the cells were seeded in 500 μL medium and incubated for 24 h in an IBIDI 24 well plate. 1 h prior to treatment the medium was changed to 450 μL fresh medium. 50 μL of the polymer solutions were added to the cells which were then incubated for another 1 h. After the incubation the cells were washed twice with warm 1× DPBS, followed by a fixation step with a 2% prediluted paraformaldehyde solution in 1× PBS. The fixation took place at room temperature for 10 min. Afterwards, the cells were washed twice with warm 1× PBS. Hoechst 33342 and CellMask Plasma Membrane Stain green were prediluted in warm cell culture medium and added to each well (0.5 μL of each stain per well). The staining was performed at 37 °C in a humidified 5% v/v CO_2 atmosphere for 10 min. Afterwards the cells were washed again twice with 1× DPBS and then measured in 1× DPBS by CLSM. Imaging was performed using the LSM980 (Zeiss). The lasers had a wavelength of 405 nm (0.2%) (detection wavelength 410–481 nm, detection of Hoechst), 488 nm (0.7%) (detection wavelength 492–527 nm, membrane) and 639 nm (1.1%) (detection wavelength 644–710 nm, detection of Cy5). All images were processed with ZEN software, version 3.7 (ZEN lite) (Zeiss).

All measurements were performed at least twice, and the images presented in the paper are representative.

4.3.7. Cell analysis *via* Cell Discoverer 7. L929 (mouse fibroblast cell line) and MDA-MB-231 (triple-negative human breast adenocarcinoma cell line) were cultured in DMEM (1 g L^{-1} glucose, supplemented with 10% (v/v) FBS, 100 U mL^{-1} penicillin, 100 μg mL^{-1} streptomycin) in an IBIDI 96-well square plate. All cell lines were cultivated at 37 °C in a humidified 5% (v/v) CO_2 incubator. 24 h prior to treatment, the cells were seeded at cell densities of 0.1 and 0.2 × 10^6 cells per mL, respectively. 1 h prior to treatment medium was replaced by 100 μL of fresh medium. 1 h after medium change, the medium got exchanged by prewarmed medium supplemented with Hoechst 33342, trihydrochloride, trihydrate to reach a final amount of 0.1 μL of Hoechst solution per well. This solution was then incubated for 10 min in the incubator at 37 °C. Afterwards, the solution was discarded and the cells were washed once with 100 μL of prewarmed 1× concentrated DPBS and immediately afterwards, 90 μL of prewarmed medium was added to the cells, followed by 10 μL of different polymer solutions (P(Lys-OH-AAM), P(Me_3Lys-OH-AAm), P(Phe-OH-AAm), P(Phenyl-OH-AAm), and P(Hex-OH-AAm) except for the control well, where 100 μL of medium were added. Final polymer solutions on cells were 2.5 μM. After adding polymers all treated wells were covered with 100 μL of IBIDI anti-evaporation oil sterile for cell culture to reduce medium evaporation during experimentation. With finalization of cell preparation, the well was moved to Carl Zeiss Cell Discoverer 7. The cells were cultivated further at 37 °C at 5% CO_2 and under a humidified atmosphere. From the first measurement on, an image has been made every 1 h for a period of 24 h. For this purpose, the autofocus function of the machine has been used to find cells on the basis of the nucleus signal. The following laser settings were applied: Hoechst 33342 has been measured at 352 nm excitation and 455 nm emission with a laser LED power of 20% for 2 ms. Cy5 signals have been measured at 650 nm excitation and 673 nm of emission at a laser LED power of 12.1% for 3 ms. Brightfield measurement took place at 10% laser power for 2.5 ms. All samples were measured with a plan-apochromat 20×/0.95 objective and 1× tubulens. The created image settings were identical for each polymer throughout different cell lines and control samples, to obtain comparable results. The measurement has been performed at least twice, and the images are representative.

4.3.8. Statistical analysis. To assess the normal distribution of the data, a Lilliefors test was conducted using Origin2025 (OriginLab, Massachusetts, USA). Afterwards, a Levene's test was performed to analyse the homogeneity of the variances. In addition, the unequal variances were tested by the unpaired Welch's *t*-test. Statistical significance was defined as $p \leq 0.05$ for all tests.

Author contributions

J. D. B. data curation, formal analysis, investigation, methodology, validation, visualisation, writing – original draft; T. M. L. data curation, formal analysis, investigation, methodology, validation, visualisation, software, supervision, writing – review and editing; C. J. data curation, formal analysis, writing – review and editing; J. P. D. data curation, formal analysis, investigation, methodology, visualisation, writing – review and editing. V. J. methodology, supervision, writing – review and editing; R. F. resources, writing – review and editing; A. T. funding acquisition, resources, supervision, writing – review and editing; M. N. L. conceptualisation, funding acquisition, methodology, project administration, resources, supervision, writing – review and editing.

Conflicts of interest

The authors declare no competing financial interest.

Data availability

The primary data are available from the corresponding author upon reasonable request.

Supplementary information (SI): further analysis of the materials in this study, including ^{1}H spectra, fluorescence spectra, FTIR spectra, HPLC data, SEC data, DLS and ELS data, cell viability data, cell association and uptake data, pK_a and log *P* calculation data. See DOI: https://doi.org/10.1039/d6tb00315j.

Acknowledgements

The authors would like to acknowledge Prof. Johannes Brendel and Prof. Thomas Scheibel for providing access to their laboratories and equipment. We thank Dr Martin Humenik for his help with the HPLC. We would like to thank Robert Bätz and Sebastian Städter for conducting size-exclusion chromatography measurements. This project was generously supported by the German Research Foundation (DFG; project number 535904448). Furthermore, funding was provided by the funding scheme Exzellenzverbünde und Universitäts-Kooperationen (EVUK) within the project ''Function by Design: Cellular Hybrids'' by the Bavarian Ministry of the Science and Art. The authors gratefully acknowledge the Bundesministerium für Bildung und Forschung (BMBF, Germany, #13XP5034A PolyBioMik), the DFG Projects PolyTarget (SFB 1278, project B01, C06, project ID: 316213987) as well as the ''Thüringer Aufbaubank (TAB)'' (2021 FGI 0005), and the ''Europäischer Fond für regionale Entwicklung (EFRE)'' (2018FGI0025) for funding of flow cytometry devices at the Jena Center for Soft Matter (JCSM). This work was performed within the Joint Lab for Polymers Jena-Bayreuth. We thank the Microverse Imaging Center (and Aurélie Jost/Patrick Then) for providing microscope facility support for data acquisition (and data analysis). The LSM 980 (used for producing images in Fig. 5) was funded by the Free State of Thuringia with the grant number 2019 FGI 0001. The Microverse Imaging Center is funded by the DFG under Germany's Excellence Strategy – EXC 2051 – Project-ID

390713860. We thank BioRender.com for the possibility of graphic creation. J. P. D. acknowledges funding through a scholarship from the Thüringer Aufbaubank and ''Europäischen Sozialfonds Plus der Europäischen Union''. The table of contents graphic was partly created with BioRender.

References

1 J. Patil, D. M. Pawde, S. Bhattacharya and S. Srivastava, Phospholipid Complex Formulation Technology for Improved Drug Delivery in Oncological Settings: A Comprehensive Review, *AAPS PharmSciTech*, 2024, **25**(5), 91.
2 S. B. Lim, A. Banerjee and H. Önyüksel, Improvement of Drug Safety by the Use of Lipid-Based Nanocarriers, *J. Controlled Release*, 2012, **163**(1), 34–45.
3 S. Chandel, P. Kumar Bolla, D. V. Bhalani, B. Nutan, A. Kumar and A. K. Singh Chandel, Bioavailability Enhancement Techniques for Poorly Aqueous Soluble Drugs and Therapeutics, *Biomedicine*, 2022, **10**, 2055.
4 Y. Zhong, F. Meng, C. Deng and Z. Zhong, Ligand-Directed Active Tumor-Targeting Polymeric Nanoparticles for Cancer Chemotherapy, *Biomacromolecules*, 2014, **15**(6), 1955–1969.
5 J. De Breuck, M. Streiber, M. Ringleb, D. Schröder, N. Herzog, U. S. Schubert, S. Zechel, A. Traeger and M. N. Leiske, Amino-Acid-Derived Anionic Polyacrylamides with Tailored Hydrophobicity-Physicochemical Properties and Cellular Interactions, *ACS Polym. Au*, 2024, **4**(3), 222–234, DOI: 10.1021/acspolymersau.3c00048.
6 M. N. Leiske, B. G. De Geest and R. Hoogenboom, Impact of the Polymer Backbone Chemistry on Interactions of Amino-Acid-Derived Zwitterionic Polymers with Cells, *Bioact. Mater.*, 2023, **24**, 524–534, DOI: 10.1016/j.bioactmat.2023.01.005.
7 E. Van Andel, S. C. Lange, S. P. Pujari, E. J. Tijhaar, M. M. J. Smulders, H. F. J. Savelkoul and H. Zuilhof, Systematic Comparison of Zwitterionic and Non-Zwitterionic Antifouling Polymer Brushes on a Bead-Based Platform, *Langmuir*, 2018, **35**(5), 1181–1191.
8 O. J. Uwaezuoke, P. Kumar, V. Pillay and Y. E. Choonara, Fouling in Ocular Devices: Implications for Drug Delivery, Bioactive Surface Immobilization, and Biomaterial Design, *Drug Delivery Transl. Res.*, 2021, **11**(5), 1903–1923.
9 M. Yessine, Membrane-Destabilizing Polyanions: Interaction with Lipid Bilayers and Endosomal Escape of Biomacromolecules, *Adv. Drug Delivery Rev.*, 2004, **56**(7), 999–1021.
10 Y. Zhang, H. F. Chan and K. W. Leong, Advanced Materials and Processing for Drug Delivery: The Past and the Future, *Adv. Drug Delivery Rev.*, 2013, **65**(1), 104–120.
11 G. Gauthier-Coles, J. Vennitti, Z. Zhang, W. C. Comb, S. Xing, K. Javed, A. Bröer and S. Bröer, Quantitative Modelling of Amino Acid Transport and Homeostasis in Mammalian Cells, *Nat. Commun.*, 2021, **12**(1), 5282.
12 D. Pei and M. Buyanova, Overcoming Endosomal Entrapment in Drug Delivery, *Bioconjugate Chem.*, 2018, **30**(2), 273–283.
13 A. A. Gabizon, Liposome Circulation Time and Tumor Targeting: Implications for Cancer Chemotherapy, *Adv. Drug Delivery Rev.*, 1995, **16**(2–3), 285–294.
14 A. L. Klibanov, K. Maruyama, V. P. Torchilin and L. Huang, Amphipathic Polyethyleneglycols Effectively Prolong the Circulation Time of Liposomes, *FEBS Lett.*, 1990, **268**(1), 235–237.
15 H. Kang, S. Rho, W. R. Stiles, S. Hu, Y. Baek, D. W. Hwang, S. Kashiwagi, M. S. Kim and H. S. Choi, Size-Dependent EPR Effect of Polymeric Nanoparticles on Tumor Targeting, *Adv. Healthcare Mater.*, 2020, **9**(1), 1901223.
16 J. Fang, H. Nakamura and H. Maeda, The EPR Effect: Unique Features of Tumor Blood Vessels for Drug Delivery, Factors Involved, and Limitations and Augmentation of the Effect, *Adv. Drug Delivery Rev.*, 2011, **63**(3), 136–151.
17 A. Traeger and M. N. Leiske, The Whole Is Greater than the Sum of Its Parts – Challenges and Perspectives in Polyelectrolytes, *Biomacromolecules*, 2024, **26**(1), 5–32.
18 M. Li, W. Zhang, J. Li, Y. Qi, C. Peng, N. Wang, H. Fan and Y. Li, Zwitterionic Polymers: Addressing the Barriers for Drug Delivery, *Chinese Chem. Lett.*, 2023, **34**(11), 108177.
19 L. S. Reichel and A. Traeger, Stimuli-Responsive Non-Viral Nanoparticles for Gene Delivery, *Handb. Exp. Pharmacol.*, 2023, **284**, 27–43.
20 P. Klemm, J. I. Solomun, M. Rodewald, M. T. Kuchenbrod, V. G. Hänsch, F. Richter, J. Rgen Popp, C. Hertweck, S. Hoeppener, C. Bonduelle, S. Lecommandoux, A. Traeger and S. Schubert, Efficient Gene Delivery of Tailored Amphiphilic Polypeptides by Polyplex Surfing, *Biomacromolecules*, 2022, **23**, 4733.
21 N. P. Ingle, J. K. Hexum and T. M. Reineke, Polyplexes Are Endocytosed by and Trafficked within Filopodia, *Biomacromolecules*, 2020, **21**(4), 1379–1392.
22 Z. U. Rehman, I. S. Zuhorn and D. Hoekstra, How Cationic Lipids Transfer Nucleic Acids into Cells and across Cellular Membranes: Recent Advances, *J. Controlled Release*, 2013, **166**(1), 46–56, DOI: 10.1016/J.JCONREL.2012.12.014.
23 P. G. Millili, J. A. Selekman, K. M. Blocker, D. A. Johnson, U. P. Naik and M. O. Sullivan, Structural and Functional Consequences of Poly(Ethylene Glycol) Inclusion on DNA Condensation for Gene Delivery, *Microsc. Res. Technol.*, 2010, **73**(9), 866–877.
24 J. I. Solomun, L. Martin, P. Mapfumo, E. Moek, E. Amro, F. Becker, S. Tuempel, S. Hoeppener, K. L. Rudolph and A. Traeger, PH-Sensitive Packaging of Cationic Particles by an Anionic Block Copolymer Shell, *J. Nanobiotechnol.*, 2022, **20**(1), 336.
25 F. Richter, L. Martin, K. Leer, E. Moek, F. Hausig, J. C. Brendel, J. C. Brendel, A. Traeger and A. Traeger, Tuning of Endosomal Escape and Gene Expression by Functional Groups, Molecular Weight and Transfection Medium: A Structure–Activity Relationship Study, *J. Mater. Chem. B*, 2020, **8**(23), 5026–5041.
26 J. I. Solomun, G. Cinar, P. Mapfumo, F. Richter, E. Moek, F. Hausig, L. Martin, S. Hoeppener, I. Nischang and A. Traeger, Solely Aqueous Formulation of Hydrophobic

Cationic Polymers for Efficient Gene Delivery, *Int. J. Pharm.*, 2021, **593**, 120080.
27 S. Fujii and K. Sakurai, Zwitterionic Amino Acid Polymer-Grafted Core-Crosslinked Particle toward Tumor Delivery, *Biomacromolecules*, 2022, **23**(9), 3968–3977.
28 S. Fujii, S. Takano, K. Nakazawa and K. Sakurai, Impact of Zwitterionic Polymers on the Tumor Permeability of Molecular Bottlebrush-Based Nanoparticles, *Biomacromolecules*, 2022, **23**(7), 2846–2855.
29 J. B. Schlenoff, Zwitteration: Coating Surfaces with Zwitterionic Functionality to Reduce Nonspecific Adsorption, *Langmuir*, 2014, **30**(32), 9625–9636.
30 M. He, K. Gao, L. Zhou, Z. Jiao, M. Wu, J. Cao, X. You, Z. Cai, Y. Su and Z. Jiang, Zwitterionic Materials for Antifouling Membrane Surface Construction, *Acta Biomater.*, 2016, **40**, 142–152, DOI: 10.1016/J.ACTBIO.2016.03.038.
31 R. Bernstein, S. Belfer and V. Freger, Bacterial Attachment to RO Membranes Surface-Modified by Concentration-Polarization-Enhanced Graft Polymerization, *Environ. Sci. Technol.*, 2011, **45**(14), 5973–5980.
32 P. Sarker, T. Lu, D. Liu, G. Wu, H. Chen, M. S. Jahan Sajib, S. Jiang, Z. Chen and T. Wei, Hydration Behaviors of Nonfouling Zwitterionic Materials, *Chem. Sci.*, 2023, **14**(27), 7500–7511, DOI: 10.1039/d3sc01977b.
33 R. Chen, M. E. Eccleston, Z. Yue and N. K. H. Slater, Synthesis and PH-Responsive Properties of Pseudo-Peptides Containing Hydrophobic Amino Acid Grafts, *J. Mater. Chem.*, 2009, **19**(24), 4217–4224.
34 S. Chen, S. Wang, M. Kopytynski, M. Bachelet and R. Chen, Membrane-Anchoring, Comb-Like Pseudopeptides for Efficient, PH-Mediated Membrane Destabilization and Intracellular Delivery, *ACS Appl. Mater. Interfaces*, 2017, **9**(9), 8021–8029.
35 A. Laschewsky, Structures and Synthesis of Zwitterionic Polymers, *Polymers*, 2014, **6**(5), 1544–1601.
36 S. Wang, PH-Responsive Amphiphilic Carboxylate Polymers: Design and Potential for Endosomal Escape, *Front. Chem.*, 2021, **9**, 1–8.
37 S. Takano, K. Sakurai and S. Fujii, Internalization into Cancer Cells of Zwitterionic Amino Acid Polymers via Amino Acid Transporter Recognition, *Polym. Chem.*, 2021, **12**(42), 6083–6087.
38 I. Theodorou, P. Anilkumar, B. Lelandais, D. Clarisse, A. Doerflinger, E. Gravel, F. Ducongé and E. Doris, Stable and Compact Zwitterionic Polydiacetylene Micelles with Tumor-Targeting Properties, *Chem. Commun.*, 2015, **51**(80), 14937–14940.
39 M. N. Leiske and K. Kempe, A Guideline for the Synthesis of Amino-Acid-Functionalized Monomers and Their Polymerizations, *Macromol. Rapid Commun.*, 2022, **43**(2), 1–24.
40 T. Maji, S. Banerjee, Y. Biswas and T. K. Mandal, Dual-Stimuli-Responsive l -Serine-Based Zwitterionic UCST-Type Polymer with Tunable Thermosensitivity, *Macromolecules*, 2015, **48**(14), 4957–4966.
41 K. Bauri, S. G. Roy, S. Pant and P. De, Controlled Synthesis of Amino Acid-Based PH-Responsive Chiral Polymers and Self-Assembly of Their Block Copolymers, *Langmuir*, 2013, **29**(8), 2764–2774.
42 J. De Breuck, V. Jérôme, R. Freitag and M. N. Leiske, Zwitterionic Amino-Acid-Derived Polyacrylamides with a Betaine Twist – Synthesis and Characterization, *Macromol. Rapid Commun.*, 2025, **46**(1), 2400623.
43 M. Namazian and S. Halvani, Calculations of PKa Values of Carboxylic Acids in Aqueous Solution Using Density Functional Theory, *J. Chem. Thermodyn.*, 2006, **38**(12), 1495–1502, DOI: 10.1016/J.JCT.2006.05.002.
44 S. A. Wildman and G. M. Crippen, Prediction of Physicochemical Parameters by Atomic Contributions, *J. Chem. Inf. Comput. Sci.*, 1999, **39**(5), 868–873.
45 P. Kord Forooshani and B. P. Lee, Recent Approaches in Designing Bioadhesive Materials Inspired by Mussel Adhesive Protein, *J. Polym. Sci., Part A: Polym. Chem.*, 2017, **55**(1), 9–33.
46 M. C. Dawson; D. C. Elliott; W. H. Elliott and K. Jones, *M.data for biochemical research*, Clarendon Press, Oxford, 1959.
47 R. van Sluis, Z. M. Bhujwalla, N. Raghunand, P. Ballesteros, J. Alvarez, S. Cerdn, J.-P. Galons and R. J. Gillies, *In Vivo* Imaging of Extracellular PH Using1H MRSI, *Magn. Reson. Med.*, 1999, **41**(4), 743–750.
48 P. Dinda, M. Anas, P. Banerjee and T. K. Mandal, Dual Thermoresponsive Boc-Lysine-Based Acryl Polymer: RAFT Kinetics and Anti-Protein-Fouling of Its Zwitterionic Form, *Macromolecules*, 2022, **55**(10), 4011–4024.
49 Y. N. Chou and M. Z. Ou, Zwitterionic Surface Modification of Aldehydated Sulfobetaine Copolymers for the Formation of Bioinert Interfaces, *ACS Appl. Polym. Mater.*, 2023, **5**(7), 5411–5428.
50 Z. Wang, G. Ma, J. Zhang, W. Lin, F. Ji, M. T. Bernards and S. Chen, Development of Zwitterionic Polymer-Based Doxorubicin Conjugates: Tuning the Surface Charge To Prolong the Circulation and Reduce Toxicity, *Langmuir*, 2014, **30**(13), 3764–3774.
51 H. Ou, T. Cheng, Y. Zhang, J. Liu, Y. Ding, J. Zhen, W. Shen, Y. Xu, W. Yang, P. Niu, J. Liu, Y. An, Y. Liu and L. Shi, Surface-Adaptive Zwitterionic Nanoparticles for Prolonged Blood Circulation Time and Enhanced Cellular Uptake in Tumor Cells, *Acta Biomater.*, 2018, **65**, 339–348.
52 M. N. Leiske, C. Kuenneth, J. De Breuck, B. G. De Geest and R. Hoogenboom, Amphiphilic Zwitterionic Bioderived Block Copolymers from Glutamic Acid and Cholesterol – Ability to Form Nanoparticles and Serve as Vectors for the Delivery of 6-Mercaptopurine, *Macromol. Chem. Phys.*, 2023, **224**(24), 1–11.
53 M. N. Leiske, Z. A. I. Mazrad, A. Zelcak, K. Wahi, T. P. Davis, J. A. McCarroll, J. Holst and K. Kempe, Zwitterionic Amino Acid-Derived Polyacrylates as Smart Materials Exhibiting Cellular Specificity and Therapeutic Activity, *Biomacromolecules*, 2022, **23**(6), 2374–2387.
54 Y. Qu, B. Han, Y. Yu, W. Yao, S. Bose, B. Y. Karlan, A. E. Giuliano and X. Cui, Evaluation of MCF10A as a Reliable Model for Normal Human Mammary Epithelial Cells, *PLoS One*, 2015, **10**(7), e0131285.

55 Y. Zhang, M. Yang, J. H. Park, J. Singelyn, H. Ma, M. J. Sailor, E. Ruoslahti and M. Ozkan, Ozkan, C. A Surface-Charge Study on Cellular-Uptake Behavior of F3- Peptide-Conjugated Iron Oxide Nanoparticles, *Small*, 2009, **5**(17), 1990–1996.

56 M. Ghirardello, R. Shyam and M. C. Galan, Reengineering of Cancer Cell Surface Charges Can Modulate Cell Migration, *Chem. Commun.*, 2022, **58**(36), 5522–5525.

57 M. Morotti, C. E. Zois, R. El-Ansari, M. L. Craze, E. A. Rakha, S. J. Fan, A. Valli, S. Haider, D. C. I. Goberdhan, A. R. Green and A. L. Harris, Increased Expression of Glutamine Transporter SNAT2/SLC38A2 Promotes Glutamine Dependence and Oxidative Stress Resistance, and Is Associated with Worse Prognosis in Triple-Negative Breast Cancer, *Br. J. Cancer*, 2020, **124**(2), 494–505.

58 S. Kwon, S. J. Han and K. S. Kim, Differential Response of MDA-MB-231 Breast Cancer and MCF10A Normal Breast Cells to Cytoskeletal Disruption, *Oncol. Rep.*, 2023, **50**(5), 1–12.

59 H. E. Davis, M. Rosinski, J. R. Morgan and M. L. Yarmush, Charged Polymers Modulate Retrovirus Transduction via Membrane Charge Neutralization and Virus Aggregation, *Biophys. J.*, 2004, **86**(2), 1234–1242.

60 J. R. Kitchen and R. L. Cysyk, Synthesis and Release of Hyaluronic Acid by Swiss 3T3 Fibroblasts, *Biochem. J.*, 1995, **309**(2), 649–656.

61 E. A. Dailing, K. V. Kilchrist, J. W. Tierney, R. B. Fletcher, B. C. Evans and C. L. Duvall, Modifying Cell Membranes with Anionic Polymer Amphiphiles Potentiates Intracellular Delivery of Cationic Peptides, *ACS Appl. Mater. Interfaces*, 2020, **12**(45), 50222–50235.

62 B. C. Evans, R. B. Fletcher, K. V. Kilchrist, E. A. Dailing, A. J. Mukalel, J. M. Colazo, M. Oliver, J. Cheung-Flynn, C. M. Brophy, J. W. Tierney, J. S. Isenberg, K. D. Hankenson, K. Ghimire, C. Lander, C. A. Gersbach and C. L. Duvall, An Anionic, Endosome-Escaping Polymer to Potentiate Intracellular Delivery of Cationic Peptides, Biomacromolecules, and Nanoparticles, *Nat. Commun. 2019 101*, 2019, **10**(1), 5012.

63 L. M. Bareford and P. W. Swaan, Endocytic Mechanisms For Targeted Drug Delivery, *Adv. Drug Delivery Rev.*, 2007, **59**(8), 748.

64 Z. Kaźmierczak, K. Szostak-Paluch, M. Przybyło, M. Langner, W. Witkiewicz, N. Jędruchniewicz and K. Dąbrowska, Endocytosis in Cellular Uptake of Drug Delivery Vectors: Molecular Aspects in Drug Development, *Bioorg. Med. Chem.*, 2020, **28**(18), 115556.

65 M. Sousa De Almeida, E. Susnik, B. Drasler, P. Taladriz-Blanco, A. Petri-Fink and B. Rothen-Rutishauser, Understanding Nanoparticle Endocytosis to Improve Targeting Strategies in Nanomedicine, *Chem. Soc. Rev.*, 2021, **50**(9), 5397–5434.

66 S. Bröer, Amino Acid Transporters as Targets for Cancer Therapy: Why, Where, When, and How, *Int. J. Mol. Sci.*, 2020, **21**(17), 1–20.

67 B. C. Fuchs and B. P. Bode, Amino Acid Transporters ASCT2 and LAT1 in Cancer: Partners in Crime?, *Semin. Cancer Biol.*, 2005, **15**(4), 254–266.

68 Y. J. Cha, E. S. Kim and J. S. Koo, Amino Acid Transporters and Glutamine Metabolism in Breast Cancer, *Int. J. Mol. Sci.*, 2018, **19**, 907.

69 A. M. Mahmoud, P. A. J. M. de Jongh, S. Briere, M. Chen, C. J. Nowell, A. P. R. Johnston, T. P. Davis, D. M. Haddleton and K. Kempe, Carboxylated Cy5-Labeled Comb Polymers Passively Diffuse the Cell Membrane and Target Mitochondria, *ACS Appl. Mater. Interfaces*, 2019, **11**(34), 31302–31310.

70 M. van Geldermalsen, L.-E. Quek, N. Turner, N. Freidman, A. Pang, Y. F. Guan, J. R. Krycer, R. Ryan, Q. Wang and J. Holst, Benzylserine Inhibits Breast Cancer Cell Growth by Disrupting Intracellular Amino Acid Homeostasis and Triggering Amino Acid Response Pathways, *BMC Cancer*, 2018, **18**(1), 689.

71 D. K. Kim, I. J. Kim, S. Hwang, J. H. Kook, M. C. Lee, B. A. Shin, C. S. Bae, J. H. Yoon, S. G. Ahn, S. A. Kim, Y. Kanai, H. Endou and J. K. Kim, System L-Amino Acid Transporters Are Differently Expressed in Rat Astrocyte and C6 Glioma Cells, *Neurosci. Res.*, 2004, **50**(4), 437–446.

72 O. Yanagida, Y. Kanai, A. Chairoungdua, D. K. Kim, H. Segawa, T. Nii, S. H. Cha, H. Matsuo, J. I. Fukushima, Y. Fukasawa, Y. Tani, Y. Taketani, H. Uchino, J. Y. Kim, J. Inatomi, I. Okayasu, K. I. Miyamoto, E. Takeda, T. Goya and H. Endou, Human L-Type Amino Acid Transporter 1 (LAT1): Characterization of Function and Expression in Tumor Cell Lines, *Biochim. Biophys. Acta, Biomembr.*, 2001, **1514**(2), 291–302.

73 T. J. Paul, A. K. Strzelczyk, M. I. Feldhof and S. Schmidt, Temperature-Switchable Glycopolymers and Their Conformation-Dependent Binding to Receptor Targets, *Biomacromolecules*, 2020, **21**(7), 2913–2921.

74 C. J. Ferguson, R. J. Hughes, D. Nguyen, B. T. T. Pham, R. G. Gilbert, A. K. Serelis, C. H. Such and B. S. Hawkett, *Ab Initio* Emulsion Polymerization by RAFT-Controlled Self-Assembly, *Macromolecules*, 2005, **38**(6), 2191–2204.

75 Amino acid properties. https://www.peptideweb.com/amino-acid-properties.

76 R. Williams, *PKa Data Compiled*, 2022, https://organicchemistrydata.org/hansreich/resources/pka/pka_data/pka-compilation-williams.pdf.

77 J. A. Riddick; W. B. Bunger and T. K. Sakano, *Techniques of Chemistry 4th Ed, VolumeII. Organic Solvents*, John Wiley & Sons, Ltd, 1985.

78 *3-Phenylpropionic Acid*. https://go.drugbank.com/drugs/DB02024.

79 H. Ohshima, A Simple Expression for Henry's Function for the Retardation Effect in Electrophoresis of Spherical Colloidal Particles, *J. Colloid Interface Sci.*, 1994, **168**(1), 269–271.

80 Y. K. Chong, G. Moad, E. Rizzardo and S. H. Thang, Thiocarbonylthio End Group Removal from RAFT-Synthesized Polymers by Radical-Induced Reduction, *Macromolecules*, 2007, **40**(13), 4446–4455.